Cell-Free Bistatic Backscatter Communication: Channel Estimation, Optimization, and Performance Analysis

Diluka Galappaththige, *Member, IEEE*, Fatemeh Rezaei, *Member, IEEE*, Chintha Tellambura, *Fellow, IEEE,* Amine Maaref, *Senior Member, IEEE*

***Abstract*—This study introduces and investigates the integration of a cell-free architecture with bistatic backscatter communication (BiBC), referred to as cell-free BiBC or distributed access point (AP)-assisted BiBC, which can enable potential applications in future (EH)-based Internet-of-Things (IoT) networks. To that purpose, we first present a pilot-based channel estimation scheme for estimating the direct, cascaded, and forward channels. Next, we utilize the channel estimates to design the optimal beamforming weights at the APs, reflection coefficients at the tags, and reception filters at the reader to maximize the tag sum rate while meeting the tags' minimum energy requirements. Because the proposed maximization problem is non-convex, we propose a solution based on alternative optimization, fractional programming, and Rayleigh quotient techniques. We also quantify the computational complexity of the developed algorithms. Finally, we present extensive numerical results to validate the proposed channel estimation scheme and optimization framework, as well as the performance of the integration of these two technologies. Our algorithm yields impressive gains compared to the random beamforming/combining benchmark. For example, it achieves $\sim 64.8\,\%$ and $\sim 253.5\,\%$ gains in harvested power and tag sum rate, respectively, for $10\,\mathrm{dBm}$ with 36 APs and 3 tags.**

***Index Terms*—Backscatter communication systems, Semi-passive tags, Channel estimation, Resource allocation.**

I. Introduction

With the rapid deployment of fifth-generation (5G) and beyond 5G communication networks, energy harvesting (EH)-based Internet-of-Things (IoT) is becoming an extremely active research area, and the third-generation partnership project (3GPP) has launched a new study item [1]–[3]. These research items identify the following essential aspects and aims of EH-based IoT networks:

- Use cases such as identification, tracking, monitoring, actuating, and sensing for logistics, transportation, and healthcare applications.
- Exploring public/private networks, indoor/outdoor environments, macro/micro/pico cells, cell-free connectivity to user equipment (UEs) with or without relay/UE assistance, and frequency bands (licensed and unlicensed).
- Establishing EH techniques, connectivity requirements, and positioning accuracy.

These challenges open a vast array of research questions. Very few of those have been explored [4], [5]. Inspired by them, we consider the problem of supporting the energy needs of multiple tags over a large coverage area such as a warehouse with a bistatic backscatter communication (BiBC) network of dedicated access points (APs)/radio frequency (RF) sources (see Fig. 1). Furthermore, these inexpensive backscatter tag-assisted IoT networks have numerous applications, including logistics, inventory management, warehousing, manufacturing, energy industry, healthcare, agriculture, aerospace and defense, farming, retail, sports, and many more. The potential market will grow at an exponential rate; for example, parcel volume in China will reach 163.4 billion by 2025 and 220-262 billion globally by 2026 [1]–[3]. These possible use cases offer significant market opportunities.

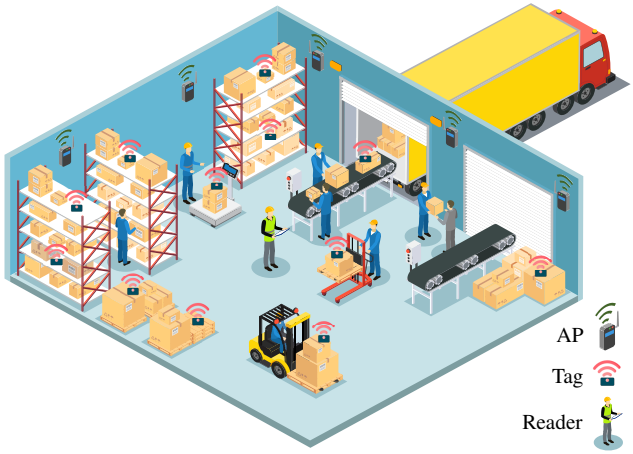

Fig. 1: A warehouse use case of cell-free BiBC network.

In scenarios like those mentioned, backscatter tags are favored due to their cost-effectiveness and minimal energy consumption (a few nW-μW). They reflect RF signals from the RF source to transmit data to a reader, whether it is a dedicated or cooperative one [4]–[6], thus optimizing spectrum utilization and reducing the need for additional spectrum allocations. Tags find utility in IoT networks, enhancing spectrum and energy efficiency [4]–[6]. Among the three backscatter network types (monostatic, bistatic, and ambient) [4], [5], BiBC systems excel in applications like warehouses. These systems employ dedicated RF sources, single or multiple, to power tags and enable backscatter modulation [4], [5]. In the context of BiBC, dedicated RF sources offer advantages over ambient signals, including predictability, reduced interference, system control, and knowledge of source signal parameters.

D. Galappaththige, F. Rezaei, and C. Tellambura with the Department of Electrical and Computer Engineering, University of Alberta, Edmonton, AB, T6G 1H9, Canada (e-mail: {diluka.lg, rezaeidi, ct4}@ualberta.ca).

A. Maaref is with Huawei Canada, 303 Terry Fox Drive, Suite 400, Ottawa, Ontario K2K 3J1 (e-mail: amine.maaref@huawei.com).

These advantages can be harnessed to optimize system coverage and performance [4], [5].

A. Technical Challenges in BiBC

Despite their wide application potential, several critical challenges constrain the performance of BiBC systems.

1) First, the dedicated RF sources (power beacons) in BiBC are primarily designed to provide energy wirelessly to tags. Power beacons offer localized coverage, providing energy within a specific area. Tags have EH circuits to convert the dedicated RF signals to direct current [4]. Specifically, the performance of the EH circuits depends on the activation threshold, typically around $-20\,\mathrm{dBm}$ [7] or more of incident RF power. Hence, depending on the proximity to the power beacon, tags may not receive adequate power to activate EH and perform data backscattering. This causes energy outages at the tags and short activation ranges (a few meters). Hence, a single power beacon supporting multiple tags limits the tag performance while increasing the probability of an energy outage. Consequently, supporting many tags across a broader area may need multiple power beacons.
2) Second, as tags backscatter their data, tag signals experience double path losses and deeper fading, leading to short communication distances ($\leq 6\,\mathrm{m}$), low data rates ($\leq 1\,\mathrm{bps/Hz}$), and low reliability [4], [5]. While connecting multiple tags is vital in applications, mutual interference caused by concurrent tag transmissions degrades the network performance. Hence, sophisticated signal processing techniques, e.g., beamforming design, interference cancellation schemes, and multiple access schemes, are essential to increase reliability while establishing massive connectivity.
3) Third, optimal beamforming design, effective suppression of the direct link interference from the power beacon, and accurate data decoding of tags depend on the availability of perfect channel state information (CSI). However, the inherent limitations in tags' power and processing capabilities, which simply backscatter incident RF signals, introduce substantial challenges to the channel estimation process. This complexity is further compounded in scenarios involving multiple power beacons and multiple tags. Thus, sophisticated methods are required for precise estimation of the direct channel ($\mathbf{h}_{0,m}$), forward channel ($f_{k,m}$), and the cascaded channels ($f_{k,m}\mathbf{g}_k$) – Fig. 2.

B. Motivation and Our Contributions

Inspired by the aforementioned challenges and significant gaps in the literature to address the needs of EH-based IoT networks, we propose supporting multiple tags over a large coverage area, such as a warehouse, with a BiBC network of dedicated distributed APs, i.e., a cell-free BiBC system.

The basic concept behind cell-free networks is that many spatially distributed APs serve multiple users on the same time-frequency resources. It thus minimizes transmission distances while increasing coverage, increasing macro-diversity and favorable propagation [8]–[10]. Hence, by shortening AP-tag distances, the cell-free architecture can alleviate the limited energy availability and adverse path loss effects in BiBC [11]–[14]. Also, a central processing unit (CPU) coordinates the APs connected to it via a front-haul/back-haul link, allowing the APs to serve users in the area collaboratively. The distributed APs in the BiBC network can thus employ the jointly designed beamforming weights to deliver as much power to the tags as possible while minimizing inter-tag interference to support many tags.

Integrating cell-free architecture with BiBC poses several critical technical challenges, such as (i) channel estimation, (ii) enabling multi-tag transmission, (iii) AP beamforming strategies, (iv) tags' reflection coefficients/power allocation, (v) designing reader reception filters, (vi) minimum energy for tag activation, (vii) coverage, (vii) coexistence with conventional cellular networks, and more. Although none of these challenges have been thoroughly investigated, [11]–[14] address some of them (Section I-C). Hence, to address these challenges while filling a significant gap in the literature, we propose a generalized cell-free BiBC system (Fig. 2).

In particular, in the channel training phase, APs operate in full-duplex (FD) mode and use a time division multiple access (TDMA) scheme, i.e., an on-off switching protocol that is controlled by the CPU, to estimate the direct (APs-reader), cascaded (APs-tags-reader), and forward (APs-tags) channels using specially designed pilot sequences. During the data transmission, the APs operate in half-duplex (HD) mode and cooperate to service the tags in the area by beamforming to improve the tags' rate performance at the reader while ensuring the tags' minimum energy requirements for tag activation. We thus design the optimal AP beamforming weights, tags' reflection coefficients, and reader's combing filters to maximize the tags' sum rate while meeting the EH requirements at the tags. We also consider the effect of estimated CSI while designing the aforementioned AP beamforming weights, tag reflection coefficients, and reader combing filters.

The main contributions of this paper can be summarized as follows:

1) Using a specifically developed pilot sequence presented in [15], we propose a method to estimate the channels of the cell-free BiBC system, including direct, cascaded, and forward channels. During this phase, an on-off switching protocol is adopted and the APs operate in FD mode. We thus derive least squares (LS) and minimum mean square error (MMSE) estimators for these channels.
2) Following that, we formulate the tag sum rate maximization problem by optimizing the beamforming weights at the APs, reflection coefficients at the tags, and receiver combiner at the reader, while maintaining the EH requirements at the tags. The formulated optimization problem also accounts for the estimated CSI and CSI estimation errors.
3) The resulting maximizing problem has a non-convex objective function and constraints. Convex problems, on the other hand, can be solved efficiently with polynomial convergence time using readily available and

widely accessible convex solvers. Therefore, we use the alternating optimization (AO) technique to decouple the non-convex problem into three sub-problems. Using this method, we develop solution algorithms for these sub-problems utilizing fractional programming (FP) and Rayleigh ratio quotient approaches.

4) We show that the proposed channel estimation scheme and optimization frameworks improve backscatter tag performance significantly in cell-free BiBC. We also investigate the algorithms' robustness to CSI errors and the computational complexities.
5) We also investigate the effects of fixed reflection coefficients at the tags. In particular, while these tags have lower performance than reconfigurable tags, i.e., tags with variable reflection coefficients, they could be a low-cost networking solution for particular applications.
6) Finally, we provide comprehensive numerical examples that demonstrate the performance of the proposed channel estimation scheme and cell-free BiBC network using the proposed solution.

Before proceeding to the technical contributions, we provide an overview of related works that attempt to address the BiBC problems outlined in Section I-A.

C. Previous Contribution on BiBC Systems

While no prior literature thoroughly addresses all the BiBC challenges, previous studies [12], [14], [16]–[18] tackled some of them. In particular, [12], [14] utilize distributed RF sources to extend the coverage distance, thereby overcoming the tag's power limitations. Reference [12] specifically investigates the placement of power beacons to maximize the coverage distance by considering the outage probability. In contrast, [14] explores tag-to-tag communication and investigates the performance of network coverage and capacity. These works, however, consider single antenna nodes and overlook the importance of beamforming designs.

On the other hand, references [16]–[18] focus on the performance studies of a BiBC with a single tag and a single RF source. In particular, [16] modifies the tag architecture to adjust the circuit load impedance of the tag to extend the communication range and lower the integrated circuit power consumption. The works [17], [18] develop interference cancellation schemes to suppress the direct link interference from the RF source, thereby improving the tag's rate. [17] uses beamforming to nullify the direct link interference. In contrast, [18] explores the joint waveform design at the RF source and coding at the tag to mitigate direct link interference. To further support multiple tags, [19] and [20] respectively adopt non-orthogonal multiple access (NOMA) and TDMA schemes. [19] maximizes the minimum tag rate by optimizing transmit beamforming at the source, receive beamforming at the reader, and reflection coefficients at the tags. Whereas [20] minimizes the transmit power level/energy consumption at the emitter by jointly optimizing the transmission time slot duration and tag reflection coefficients. Reference [21] also investigates the emitter power allocation and energy consumption, considering a separate reader for each tag. Additionally,

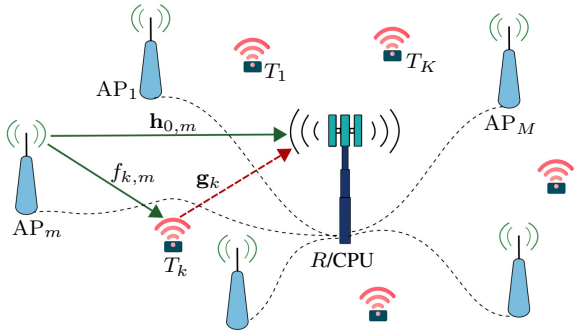

Fig. 2: Cell-free BiBC setup.

[22] designs the tag's signaling matrix to improve the bit-error-rate performance and estimate channels for a multi-antenna tag (e.g., K-antenna tag) system. In particular, to estimate the channels for each tag antenna, [22] uses the silent protocol, in which one antenna transmits a pilot sequence of length N_s at a time while others remain silent. It thus requires K^2+1 pilot sequences and $(K^2+1)N_s$ channel training duration. Nonetheless, the sequence length must be at least 100 to achieve an acceptable performance, i.e., $N_s \geq 100$, resulting in longer channel training duration.

Leveraging the concept of distributed RF sources, the authors in [13] and [11] further explore beamforming design at distributed cellular APs serving a cellular user and a tag. They also consider channel estimation through pilot transmissions from the cellular APs. Channel estimation has also been investigated in BiBC using a pilot-based two-phase channel estimation protocol [17], [23]. However, no method exists for estimating the channels of a generalized BiBC network comprising multiple RF sources, multiple tags, and a reader.

The most relevant works are summarized in Table I, highlighting the unique contribution of this paper.

D. Structure and Notation

This paper is organized as follows: Section II first introduces the system model, channel model, and EH at the tags. Next, it discusses pilot transmission and channel estimation. Further, it presents the data transmission model and the achievable rates of the tags. In Section III, we formulate the sum rate maximization problem. We present the AO solution for the proposed problem in Section IV. In Section V, simulation examples are presented for performance evaluations. Section VI concludes the paper and outlines future research directions.

Notation: Lowercase bold and uppercase bold denote vectors and matrices. $\mathbf{I}_n$ is the $n \times n$ identity matrix. $\mathbf{A}^{\mathrm{T}}$ and $\mathbf{A}^{\mathrm{H}}$, denote transpose and Hermitian transpose, respectively. $\mathbb{E}\{\cdot\}$ denotes the statistical expectation. Finally, $\mathcal{CN}(\boldsymbol{\mu}, \mathbf{R})$ is a complex Gaussian vector with mean $\boldsymbol{\mu}$ and co-variance matrix $\mathbf{R}$. Finally, $\mathcal{M} = \{1, \ldots, M\}$, $\mathcal{K} = \{1, \ldots, K\}$, and $\mathcal{K}_k = \mathcal{K} \setminus \{k\}$.

II. System, Channel, and Signal Models

A. System Model

We consider a cell-free BiBC system with M dedicated hybrid access point (H-AP), denoted by $\mathrm{AP}_m, m \in \mathcal{M}$, K

TABLE I: Summary of related works.

Conf.	Ref.	Setup			Objective	EH Constraint	Variables†	Methodology	CSI Estimation
		APs	Tags	Reader					
AmBC	[11]	$M \geq 1$	$K = 1$	$L = 1$	Tag's rate	✗	$\mathbf{w}$	SCA	✓
BiBC	[12]	$M \geq 1$	$K \geq 1$	$L = 1$	Coverage distance	✗	AP location	–	✗
	[19]‡	$M = 1$	$K \geq 1$	$L \geq 1$	Minimum Tag rate	✗	$\mathbf{w}, \mathbf{u}, \boldsymbol{\alpha}$	AO & SCA	✗
	[20]	$M = 1$	$K \geq 1$	$L = 1$	Transmit power	✓	p_t, α	SCA & BCD	✗
	[21]	$M = 1$	$K \geq 1$	$L = 1$	Energy efficiency	✓	p_t, α	Lagrange dual decomposition	✗
	This paper	$M \geq 1$	$K \geq 1$	$L \geq 1$	Tags' sum rate	✓	$\mathbf{w}, \mathbf{u}, \boldsymbol{\alpha}$	AO & FP & Rayleigh ratio quotient	✓

† The variables p_t, $\mathbf{w}$, $\mathbf{u}$, and α, denote transmit power, transmit beamforming, reception filter, and reflection coefficient. SCA - successive convex approximation. BCD - block coordinated decent.
‡ This work adopts NOMA to establish multiple access.

single-antenna tags, denoted by $T_k, k \in \mathcal{K}$, and a L-antenna reader, denoted by R (Fig. 2). Each H-AP equipped with a single antenna operates in either FD or HD mode [24]. Specifically, in FD mode, the antenna of an H-AP simultaneously excites a carrier signal and receives signals reflected by tags. We assume the FD operation with perfect self-interference cancellation at the H-AP's decoupler [25]–[27]. Each tag modulates its data on the RF signals transmitted by the H-APs and transmits the modulated signals to the reader. We assume that the reader comprises a CPU connected to all H-APs via a front-haul/back-haul link [28]. Hence, this front-haul/back-haul connection assists in sharing the necessary CSI between the reader and the H-APs. It also assists in synchronizing all APs to simultaneously serve all tags in the same time-frequency resource block by adopting spatial multiplexing rendered by cell-free massive multiple-input multiple-output (MIMO).

B. Channel Model

We consider a block flat-fading channel model. During each fading block, $\mathbf{h}_{0,m} = [h_{0,1m}, \ldots, h_{0,Lm}]^{\mathrm{T}} \in \mathbb{C}^{L\times 1}$, $f_{k,m} \in \mathbb{C}$, and $\mathbf{g}_k = [g_{1k}, \ldots, g_{Lk}]^{\mathrm{T}} \in \mathbb{C}^{L\times 1}$ denote the channels between $\mathrm{AP}_m - R$, $\mathrm{AP}_m - T_k$, and $T_k - R$, respectively. Moreover, $\mathbf{h}_{k,m} = f_{k,m}\mathbf{g}_k \in \mathbb{C}^{L\times 1}$ denotes the cascaded channel between $\mathrm{AP}_m - T_k - R$. A unified representation of all individual channels is given as

$$v = \alpha_v \exp(j\phi_v), \tag{1}$$

where $v \in \{h_{0,lm}, f_{k,m}, g_{lk}\}$ for $m \in \mathcal{M}$, $l \in \mathcal{L}$, and $k \in \mathcal{K}$. In (1), $\phi_v \in [-\pi, \pi]$ is the phase of v and α_v is the envelope of v, which is assumed to be Nakagami-$\bar{m}_v$ distributed with $\bar{m}_v$ shape and $\Omega_v = \bar{m}_v\zeta_v$ scaling parameters. Here, ζ_v captures the large-scale path loss and shadowing, which stays constant for several coherence intervals. Hence, the channel statistics at the H-APs and reader are assumed to be known a-prior since they change very slowly [28].

Remark 1. *Nakagami-m is a versatile model that can describe various propagation conditions. For example, when $m = 1$, it represents Rayleigh fading, and when $m \to \infty$, it represents no fading. As a result, our proposed channel estimation and resource allocation/optimization frameworks can be applied to any fading channel, such as Rayleigh, Rician, and others [29], [30].*

In this paper, high-mobility communication scenarios are not considered. The reason is that emerging backscatter networks in the 3GPP standards focus on application scenarios such as warehouses, agriculture, and similar environments with low-mobility devices/tags. An additional goal is to keep tags inexpensive (e.g., less than a dollar each) so that they can be used to track stationery goods [1]–[3]. Thus, these are extremely low-mobility environments. Consequently, we employ the block/flat-fading channel model. Nevertheless, the proposed frameworks are still applicable in cases with some mobility given flat-fading channels. On the other hand, for high-mobility scenarios, more research is needed on channel modeling and signal processing techniques [31], [32].

C. EH at Tags

In our system, tags are assumed to be semi-passive tags with small energy storage [33]. This allows tags to only use the stored energy during the channel estimation phase. Otherwise, in the data transmission phase, tags harvest energy and send data simultaneously via the power-splitting mode [33].

Thus, during the data transmission phase, T_k reflects $\alpha_k P_k$ to send data and absorbs $P_k^{\mathrm{in}} = (1 - \alpha_k)P_k$, for EH, where P_k is incident RF power and $\alpha_k \in (0, 1)$ is the reflection coefficient of T_k. The EH circuit converts P_k^{in} to direct current power to perform internal operations and refill the energy storage [4]. The amount of harvested power at T_k, $P_{h,k}$, can be modeled as a linear or nonlinear function of the incident RF power. The linear model is the most widely used in the literature due to its simplicity, but it ignores the non-linear characteristics of actual EH circuits, such as saturation and sensitivity. For that reason, several non-linear models have been developed [34]. In particular, for the nonlinear model, $P_{h,k} = \Phi(P_k^{in})$, where $\Phi(.)$ is the nonlinear EH function [35, *Eqn. (2)*], and for the linear model, $P_{h,k} = \eta_b P_k^{in}$, where $\eta_b \in (0, 1]$ is the power conversion efficiency, which is typical $\eta_b = \{0.2, 0.4, 0.6\}$ [33]. Fortunately, as we show next, both liner and non-liner models can be handled under a single unified framework.

To activate the tag, the harvested power should exceed the threshold, i.e., $P_{h,k} \geq p_b$. The threshold is about $-20\,\mathrm{dBm}$ for commercial passive tags [4]. In particular, $P_k^{\mathrm{in}} \geq p_b'$, where $p_b' \triangleq \Phi^{-1}(p_b)$ for nonlinear EH model and $p_b' = p_b/\eta_b$ for linear EH case.

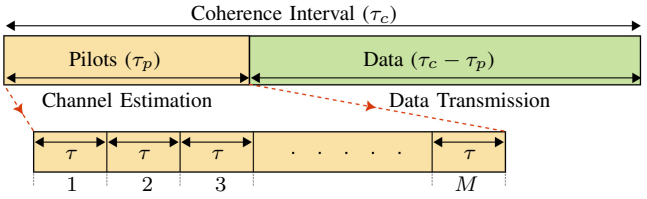

Fig. 3: Transmission framework.

D. Pilot Transmission and Channel Estimation

In our study, we adopt a cell-free BiBC system operating in the time division duplex (TDD) transmission mode for both channel estimation and data transmission [36]. TDD, a widely used multiple-access technique, allocates distinct time slots for uplink and downlink transmissions over a single channel. This characteristic makes TDD an efficient choice in spectrum utilization [37], as it allows dynamic allocation of time slots without needing to modify the bandwidth. This flexibility is beneficial in meeting diverse application requirements and ensuring the quality of service [37], making TDD particularly suitable for scenarios with unpaired spectrum and asymmetric data rate needs. One of the advantages of TDD over frequency division duplex (FDD) is its simplified channel equalization methods, emanating from the principle of channel reciprocity [37]. This simplification reduces the complexity of the system while maintaining reliable communication performance. In sum, Our choice of TDD for the cell-free BiBC system is justified by its spectrum efficiency, dynamic resource allocation, and simplicity compared to FDD [37].

Accurate estimation of the channels is necessary to benefit from cell-free BiBC fully. In particular, the CSI of forward channels, i.e., $f_{k,m}$ for $m \in \mathcal{M}$ and $k \in \mathcal{K}$, and the cascaded channels, i.e., $\mathbf{h}_{k,m}$ for $m \in \mathcal{M}$ and $k \in \mathcal{K}$, is crucial for designing beamforming at APs, reflection coefficients at tags, and reception filters at the reader while guaranteeing EH and rate performance. On the other hand, the reader requires accurate information about the direct channels, i.e., $\mathbf{h}_{0,m}$ for $m \in \mathcal{M}$, to suppress the direct link interference before decoding the tags' data. By accurately estimating these channels, the BiBC system's performance can be enhanced by improving signal quality and successfully decoding data transmitted by tags.

Following the methodology presented in [15], we employ a pilot-based channel estimation scheme to estimate $\mathbf{h}_{0,m}$, $\mathbf{h}_{k,m}$, and $f_{k,m}$ for $m \in \mathcal{M}$ and $k \in \mathcal{K}$. We assume that in each coherence block of length τ_c, $\tau_p (< \tau_c)$ samples are used for channel estimation (Fig. 3). During the channel estimation phase, we adopt a TDMA scheme, using an on-off switching protocol controlled by the CPU. Specifically, the channel estimation duration τ_p is divided into M slots, each with length $\tau \geq K+1$, and $\tau_p = M\tau$. In each time slot, the CPU activates a specific AP in FD mode to transmit a pilot sequence $\mathbf{s} = [s_1, \ldots, s_\tau] \in \mathbb{C}^{1\times\tau}$, while the remaining APs are turned off. Here, s_i satisfies $|s_i|^2 = 1$ for $i = \{1\ldots, \tau\}$. In the given time slot, all the tags are active and backscatter the AP signal to transmit their pilot signals, i.e., T_k backscatters $\mathbf{c}_k = [c_{k1}, \ldots c_{k\tau}] \in \mathbb{C}^{1\times\tau}$, where c_{ki} is the tag's transmit pilot symbol over the ith AP symbol, s_i. The reader estimates the direct and cascaded channels using the tags' backscattered and activated AP signals. In contrast, the activated AP estimates the forward channels using the tags' backscattered signals.

Remark 2. *For evaluating channel estimation performance, we assume that the tags use modified Zadoff-Chu sequences as pilots, $\mathbf{c}_k$, as in [15]. However, other sequences, such as rows of Hadamard Matrix, can be used to estimate the channels. Furthermore, according to Theorem 4 in [15], any set of orthogonal sequences can be modified for backscatter channel estimation based on the characteristics of the tag's RF front end, the complexity of the tag itself, and the application environment.*

The received signals at the reader at the mth time slot, over τ pilot symbols, can be expressed as [15]

$$\mathbf{Y}_m = \sqrt{p_p}\mathbf{H}_m\mathbf{X}\mathbf{S} + \mathbf{N}_m, \tag{2}$$

where p_p is the pilot transmit power, $\mathbf{H}_m = [\mathbf{h}_{0,m}, \sqrt{\alpha_1}\mathbf{h}_{1,m}, \ldots, \sqrt{\alpha_K}\mathbf{h}_{K,m}] \in \mathbb{C}^{L\times(K+1)}$, $\mathbf{S} \triangleq \text{diag}(\mathbf{s})$, and $\mathbf{N}_m \in \mathbb{C}^{L\times\tau}$ is the noise matrix with i.i.d $\mathcal{CN}(0,\sigma^2)$ elements. In (2), $\mathbf{X} = [\mathbf{x}_1, \ldots, \mathbf{x}_\tau] \in \mathbb{C}^{(K+1)\times\tau}$, includes the transmitted pilots by the tags, $\mathbf{x}_i = [1, c_{1i}, \ldots, c_{Ki}]^{\mathrm{T}} \in \mathbb{C}^{(K+1)\times 1}$, and $\mathbf{X}\mathbf{X}^{\mathrm{H}} = \tau\mathbf{I}_{K+1}$.

In order to estimate $\mathbf{H}_m$, by projecting the received signal (2) onto $\mathbf{S}^{\mathrm{H}}$, the post-processed received signal is given as

$$\bar{\mathbf{Y}}_m = \sqrt{p_p}\mathbf{H}_m\mathbf{X} + \bar{\mathbf{N}}_m, \tag{3}$$

where $\bar{\mathbf{N}}_m = \mathbf{N}_m\mathbf{S}^{\mathrm{H}} \in \mathbb{C}^{L\times\tau}$ is the noise matrix with i.i.d $\mathcal{CN}(0,\sigma^2)$ elements.

The reader then correlates the received pilot signal in (3) with $\mathbf{X}$, which results in a de-spreading operation. The post-processed signal is thus given as

$$\bar{\mathbf{Y}}_{m,p} = \bar{\mathbf{Y}}_m\mathbf{X}^{\mathrm{H}}/\tau = \sqrt{p_p}\mathbf{H}_m + \bar{\mathbf{N}}_{m,p}, \tag{4}$$

where $\bar{\mathbf{N}}_{m,p} = \bar{\mathbf{N}}_m\mathbf{X}^{\mathrm{H}}/\tau$ having i.i.d $\mathcal{CN}(0,\sigma_p^2)$ elements, where $\sigma_p^2 = \sigma^2/\tau$. Given independent Rayleigh fading, the channel matrix and the noise matrix elements are statistically independent. Next, the (l,k)th element of (4) is given as

$$[\bar{\mathbf{Y}}_{m,p}]_{l,k} \triangleq y_{l,k}^m = \sqrt{p_p}h_{l,k}^m + n_{l,k}^m, \tag{5}$$

where $h_{l,k}^m = [\mathbf{H}_m]_{l,k}$ and $n_{l,k}^m = [\bar{\mathbf{N}}_{m,p}]_{l,k}$.

The MMSE estimator is thus given as (Appendix A) [15]

$$\hat{h}_{l,k}^m = \mathbb{E}\{h_{l,k}^m | y_{l,k}^m\} = \frac{\mathbb{E}\{h_{l,k}^m (y_{l,k}^m)^*\}}{\mathbb{E}\{|y_{l,k}^m|^2\}} y_{lk}^m$$
$$= \begin{cases} \frac{\sqrt{p_p}\beta_{h_{0,lm}}}{p_p\beta_{h_{0,lm}}+\sigma_p^2} y_{l0}^m, & \text{for} \quad k = 0, \\ \frac{\sqrt{\alpha_k p_p}\beta_{h_{k,lm}}}{\alpha_k p_p\beta_{h_{k,lm}}+\sigma_p^2} y_{lk}^m, & \text{for} \quad k \in \mathcal{K}, \end{cases} \tag{6}$$

where $\beta_{h_{k,lm}}$ is given as

$$\beta_{h_{0,lm}} = \frac{\Gamma(\bar{m}_{h_{0,lm}}+1)}{\Gamma(\bar{m}_{h_{0,lm}})} \frac{\Omega_{h_{0,lm}}}{\bar{m}_{h_{0,lm}}}, \tag{7a}$$

$$\beta_{h_{k,lm}} = \frac{\Gamma(\bar{m}_{f_{k,m}}+1)\Gamma(\bar{m}_{g_{lk}}+1)}{\Gamma(\bar{m}_{f_{k,m}})\Gamma(\bar{m}_{g_{lk}})} \frac{\Omega_{f_{k,m}}\Omega_{g_{lk}}}{\bar{m}_{f_{k,m}}\bar{m}_{g_{lk}}}. \tag{7b}$$

Since the reader antenna elements are co-located, the large-scale parameters are identical, i.e., $\zeta_{h_{0,lm}} = \zeta_{h_{0,m}}$, $\zeta_{g_{lk}} = \zeta_{g_k}$ for $l \in \mathcal{L}$. We thus have $\beta_{h_{0,lm}} = \beta_{h_{0,m}}$ and $\beta_{h_{k,lm}} = \beta_{h_{k,m}}$, and the MMSE estimate of the complete channel matrix, $\mathbf{H}_m$, is given as

$$\hat{\mathbf{H}}_m^{\mathrm{MMSE}} = \bar{\mathbf{Y}}_{m,p}\mathbf{D}_{m,\gamma}^{1/2}, \tag{8}$$

where $\mathbf{D}_{m,\gamma_{}} = \mathrm{diag}([\gamma_{0,m}, \gamma_{1,m}, \ldots, \gamma_{K,m}])$, in which $\gamma_{0,m} = \frac{p_p\beta_{h_{0,m}}^2}{p_p\beta_{h_{0,m}}+\sigma_p^2}$ and $\gamma_{k,m} = \frac{\alpha_k p_p \beta_{h_{k,m}}^2}{\alpha_k p_p \beta_{h_{k,m}}+\sigma_p^2}$.

Additionally, using (2), the LS estimate, which operates without any prior knowledge of the channel, is obtained as

$$\hat{\mathbf{H}}_m^{\mathrm{LS}} = \bar{\mathbf{Y}}_m\bar{\mathbf{X}}^{\dagger}, \tag{9}$$

where $\bar{\mathbf{X}}^{\dagger} = \mathbf{X}^{\mathrm{H}}(\bar{\mathbf{X}}\bar{\mathbf{X}}^{\mathrm{H}})^{-1}$ and $\bar{\mathbf{X}} = \sqrt{p_p}\mathbf{X}$.

Remark 3. *For the linear model* (5)*, the minimum variance unbiased (MVU) estimator has the identical functional form as the LS estimator* (9)*, which aims to minimize the squared distance between the provided data $y_{l,k}^m$ and the unknown variable $h_{l,k}^m$ [38, Section 14.3.5]. The Cramér-Rao lower bound (CRLB), on the other hand, is a lower bound on the variance/mean squared error (MSE) of unbiased estimators. For the linear model given in* (5)*, the MVU estimator is efficient and achieves the CRLB [15].*

Similarly, the received signal at AP_m over τ pilot symbols can be expressed as

$$\mathbf{y}_m^p = \sqrt{p_p}\sum\nolimits_{i\in\mathcal{K}}\sqrt{\alpha_i}f_{i,m}^{\mathrm{T}}f_{i,m}\mathbf{c}_i\mathbf{S} + \mathbf{n}_m. \tag{10}$$

where $\mathbf{n}_m \in \mathbb{C}^{1\times\tau} \sim \mathcal{CN}(\mathbf{0}, \sigma_a^2\mathbf{I}_\tau)$ denotes the noise at AP_m. The post-processed received signal is thus given as

$$\bar{\mathbf{y}}_m^p = \mathbf{y}_m^p\mathbf{S}^{\mathrm{H}} = \sqrt{p_p}\sum\nolimits_{i\in\mathcal{K}}\sqrt{\alpha_i}f_{i,m}^{\mathrm{T}}f_{i,m}\mathbf{c}_i + \bar{\mathbf{n}}_m, \tag{11}$$

where $\bar{\mathbf{n}}_m = \mathbf{n}_m\mathbf{S}^{\mathrm{H}}$. The received pilot signal is then projected onto the $\mathbf{c}_k^{\mathrm{H}}$ which yields

$$y_{k,m}^p = \bar{\mathbf{y}}_m^p\mathbf{c}_k^{\mathrm{H}}/\tau = \sqrt{p_p\alpha_k}f_{k,m}^{\mathrm{T}}f_{k,m} + n_{k,m}, \tag{12}$$

where $n_{k,m} = \bar{\mathbf{n}}_m\mathbf{c}_i^{\mathrm{H}}/\tau \sim \mathcal{CN}(0, \sigma_a^2/\tau)$.

Therefore, the LS estimate of $\bar{f}_{k,m} = f_{k,m}^{\mathrm{T}}f_{k,m}$ can be obtained as[1]

$$\hat{\bar{f}}_{k,m}^{\mathrm{LS}} = y_{k,m}^p/\sqrt{p_p\alpha_k}. \tag{13}$$

Hence, we can obtain an approximate estimate for the forward channel, $f_{k,m}$, using the estimates of $\bar{f}_{k,m}$, as $\hat{f}_{k,m}^{\mathrm{LS}} \approx \sqrt{\hat{\bar{f}}_{k,m}^{\mathrm{LS}}}$. Note that this forward channel estimation may cause a phase ambiguity as it involves the square root of the complex number. However, for the proposed resource allocation, a rough estimation of the forward channel is adequate as it is only required for the tags' EH constraints. Conversely, since the cascaded channel includes the forward channel and APs collectively beamform towards tags, this phase ambiguity does not harm the proposed problem formulation or solution. Our simulation findings further corroborate the validity of this argument, indicating that the proposed approach consistently results in higher power delivery to the tags (Fig. 8 and Fig. 9).

[1]For the forward link we only derive the LS estimator for brevity.

E. Transmission Model

All APs simultaneously serve the tags in HD mode in the data transmission phase. The signal transmitted at AP_m is thus given as

$$q_m = \sqrt{p_t}\sum\nolimits_{i\in\mathcal{K}} w_{i,m}s, \tag{14}$$

where p_t is the transmit power at each AP, $w_{i,m} \in \mathbb{C}$ is the spatial directivity/precoder of the signal at AP_m for T_i, and $s \sim \mathcal{CN}(0,1)$ is the carrier signal satisfying $\mathbb{E}\{|s|^2\} = 1$. The signal received at T_k is given as

$$y_k = \mathbf{f}_k^{\mathrm{T}}\mathbf{q} = \sqrt{p_t}\sum\nolimits_{i\in\mathcal{K}}\mathbf{f}_k^{\mathrm{T}}\mathbf{w}_i s, \tag{15}$$

where $\mathbf{q} = [q_1, \ldots, q_M]^{\mathrm{T}} \in \mathbb{C}^{M\times 1}$, and $\mathbf{w}_i = [w_{1i}, \ldots, w_{Mi}]^{\mathrm{T}} \in \mathbb{C}^{M\times 1}$. Moreover, $\mathbf{f}_k = [f_{k,1}, \ldots, f_{k,M}]^{\mathrm{T}} \in \mathbb{C}^{M\times 1}$ denotes the effective channel between all APs and T_k.

The tags must harvest enough power to support their internal operations. Hence, the input signal power at EH circuit of T_k must satisfy the following energy constraint (Section II-C):

$$P_k^{\mathrm{in}} = (1-\alpha_k)p_t\left|\sum\nolimits_{i\in\mathcal{K}}\mathbf{f}_k^{\mathrm{T}}\mathbf{w}_i\right|^2 \geq p_b', \tag{16}$$

where $p_b' \triangleq \Phi^{-1}(p_b)$ for nonlinear EH model and $p_b' = p_b/\eta_b$ for linear EH case. T_k harvests energy from the received signal and modulates it with its data, c_k, where c_k is the normalized backscatter symbol selected from a multi-level ($\bar{M}$-ary) modulation such that $\mathbb{E}\{|c_k|^2\} = 1$, before sending it to the reader. The received signal at the reader is given as

$$\begin{aligned}\mathbf{r} &= \sum\nolimits_{m\in\mathcal{M}}\mathbf{h}_{0,m}q_m + \sum\nolimits_{j\in\mathcal{K}}\sqrt{\alpha_j}\mathbf{g}_j y_j c_j + \mathbf{z}\\ &= \mathbf{H}_0\mathbf{q} + \sqrt{p_t}\sum\nolimits_{j\in\mathcal{K}}\sum\nolimits_{i\in\mathcal{K}}\sqrt{\alpha_j}\mathbf{g}_j\mathbf{f}_j^{\mathrm{T}}\mathbf{w}_i s c_j + \mathbf{z},\end{aligned} \tag{17}$$

where $\mathbf{H}_0 = [\mathbf{h}_{0,1}, \ldots \mathbf{h}_{0,M}] \in \mathbb{C}^{L\times M}$, and $\mathbf{z} \in \mathbb{C}^{L\times 1} \sim \mathcal{CN}(\mathbf{0}, \sigma^2\mathbf{I}_L)$ is the additive white Gaussian noise (AWGN) vector at the reader. In (17), the first term is the direct-link signals from the APs, and the second is the backscatter-link signals from tags. Note that the reader applies the digital combining vector $\mathbf{u}_k \in \mathbb{C}^{L\times 1}$ to $\mathbf{r}$ (17) for decoding the T_k's data. Specifically, depending on the computing capability of the reader (CPU), the reader can execute data decoding online or offline in the digital domain utilizing parallel or sequential processing.

Remark 4. *The reader uses successive interference cancellation to remove the direct-link signals from all APs and then applies the combining filter, $\mathbf{u}_k$ to decode T_k's signal. Because direct channels between APs and the reader are conventional cell-free one-way channels, they can be estimated more accurately, i.e., with a lower normalized mean square error than backscatter channels. Our simulation results also support the validity of this argument (Fig 4).*

Following Remark 4, we assume that the reader can perfectly remove the direct APs' signals from the received signal

(17). The post-processed signal for decoding T_k's data at the reader is thus given as

$$\begin{aligned} r_k &= \mathbf{u}_k^{\mathrm{T}}\left(\mathbf{r}-\mathbf{H}_0\mathbf{q}\right) \\ &= \underbrace{\sqrt{\alpha_k p_t}\sum\nolimits_{i\in\mathcal{K}}\mathbf{u}_k^{\mathrm{T}}\mathbf{g}_k\mathbf{f}_k^{\mathrm{T}}\mathbf{w}_i sc_k}_{\text{Desired signal}} \\ &\quad+\underbrace{\sqrt{p_t}\sum\nolimits_{j\in\mathcal{K}_k}\sum\nolimits_{i\in\mathcal{K}}\sqrt{\alpha_j}\mathbf{u}_k^{\mathrm{T}}\mathbf{g}_j\mathbf{f}_j^{\mathrm{T}}\mathbf{w}_i sc_j}_{\text{Interference from the tag}}+\underbrace{\mathbf{u}_k^{\mathrm{T}}\mathbf{z}}_{\text{Noise}}, \end{aligned} \tag{18}$$

where the first, second, and third terms in r_k are, respectively, the desired signal, interference from other tags, and effective noise at the reader.

F. Achievable Rate

This section derives the rates of the tags. Using (18), the received SINR for T_k, γ_k', at the reader is obtained as

$$\gamma_k' = \frac{\alpha_k p_t\left|\sum_{i\in\mathcal{K}}\mathbf{u}_k^{\mathrm{T}}\mathbf{g}_k\mathbf{f}_k^{\mathrm{T}}\mathbf{w}_i\right|^2|s|^2}{p_t\sum_{j\in\mathcal{K}_k}\alpha_j\left|\sum_{i\in\mathcal{K}}\mathbf{u}_k^{\mathrm{T}}\mathbf{g}_j\mathbf{f}_j^{\mathrm{T}}\mathbf{w}_i\right|^2|s|^2+\|\mathbf{u}_k\|^2\sigma^2}. \tag{19}$$

Thus, the achievable rate of T_k at the reader is given as

$$\mathcal{R}_k = \psi\mathbb{E}_s\{\log_2(1+\gamma_k')\}, \tag{20}$$

where the pre-log factor $\psi = (\tau_c-\tau_p)/\tau_c$ captures the effective portion of the coherence interval for the downlink transmission. By taking the average over s in (20), the rate of T_k is computed as[2]

$$\mathcal{R}_k = \psi\log_2(e)\left(-e^{\frac{1}{a_k+b_k}}\mathrm{E}_i\left(\frac{-1}{a_k+b_k}\right)+e^{\frac{1}{b_k}}\mathrm{E}_i\left(\frac{-1}{b_k}\right)\right), \tag{21}$$

where

$$a_k \triangleq \frac{\alpha_k p_t}{\|\mathbf{u}_k\|^2\sigma^2}\left|\sum\nolimits_{i\in\mathcal{K}}\mathbf{u}_k^{\mathrm{T}}\mathbf{g}_k\mathbf{f}_k^{\mathrm{T}}\mathbf{w}_i\right|^2, \tag{22a}$$

$$b_k \triangleq \frac{p_t}{\|\mathbf{u}_k\|^2\sigma^2}\sum\nolimits_{j\in\mathcal{K}_k}\alpha_j\left|\sum\nolimits_{i\in\mathcal{K}}\mathbf{u}_k^{\mathrm{T}}\mathbf{g}_j\mathbf{f}_j^{\mathrm{T}}\mathbf{w}_i\right|^2. \tag{22b}$$

Additionally, $\mathrm{E}_i(x) = \int_{-\infty}^{x}u^{-1}e^u du$ is the exponential integral function. Note that, $-e^{\frac{1}{x}}\mathrm{E}_i(-1/x)$ is monotonically increasing and concave function of x [36].

Remark 5. *The number of tags that can be served in the proposed system is mainly limited by the coherence interval, τ_c, but not by the number of APs. However, pilot length must be chosen carefully to strike a balance between channel estimation and data transmission. For example, with $\tau_c = 1000$, 12 tags, and 36 APs, $\tau_p = 36(12+1) = 468$, leaving $\tau_c - \tau_p = 532$, i.e., $\psi = 0.532$, for data transmission. Consequently, the coherence interval ultimately limits the system's ability to serve tags. It is worth noting that environments like warehouses exhibit very slow fading channels, where the coherence interval approaches infinity, allowing for the service of many tags [37]. However, challenges may arise in situations with a limited coherence time. Future research endeavors will explore efficient channel estimation schemes tailored for cell-free BackCom.*

[2]For $s\sim\mathcal{CN}(0,1)$, $|s|^2$ is exponentially distributed.

III. Optimization Problem Formulation

Herein, we optimize the performance of the proposed cell-free BiBC setup (Fig. 2). We aim to maximize the sum rate of the tags while ensuring the tag activation, i.e., the tags meet the minimum operational energy requirements. The optimization variables are APs' precoders, i.e., $\mathbf{w}_k$ for $k\in\mathcal{K}$, the combining filters at the reader, i.e, $\mathbf{u}_k$ for $k\in\mathcal{K}$, and the tags' reflection coefficients, i.e, α_k for $k\in\mathcal{K}$.

The sum rate maximization problem can be formulated as

$$\mathbf{P1}: \underset{\mathbf{w}_k,\mathbf{u}_k,\alpha_k,\forall k}{\text{maximize}} \sum\nolimits_{k\in\mathcal{K}}\mathcal{R}_k, \tag{23a}$$

$$\text{subject to} \sum\nolimits_{i\in\mathcal{K}}|w_{i,m}|^2\le 1, \tag{23b}$$

$$(1-\alpha_k)p_t\left|\sum\nolimits_{i\in\mathcal{K}}\mathbf{f}_k^{\mathrm{T}}\mathbf{w}_i\right|^2\ge p_b', \tag{23c}$$

$$\|\mathbf{u}_k\|^2\le 1, \tag{23d}$$

$$0<\alpha_k<1. \tag{23e}$$

Here, (23b) is the per-AP transmit power constraint, (23c) is the minimum per-tag power requirement for EH, and (23d) is the normalization constraint for the combining filter at the reader.

Remark 6. *Converting the objective function in* (23a) *to a convex form is not possible due to the associated exponential integral function in* (21)*. To get around this problem to solve the proposed sum rate maximization problem, we replace the rate of each tag, given in* (20)*, with the following bound that closely approximates the exact rate of T_k for mathematical feasibility [39]:*

$$\mathcal{R}_k \approx \psi\log_2(1+\mathbb{E}_s\{\gamma_k'\}) = \psi\log_2(1+\gamma_k), \tag{24}$$

where

$$\gamma_k = \frac{\alpha_k p_t\left|\sum_{i\in\mathcal{K}}\mathbf{u}_k^{\mathrm{T}}\mathbf{g}_k\mathbf{f}_k^{\mathrm{T}}\mathbf{w}_i\right|^2}{p_t\sum_{j\in\mathcal{K}_k}\alpha_j\left|\sum_{i\in\mathcal{K}}\mathbf{u}_k^{\mathrm{T}}\mathbf{g}_j\mathbf{f}_j^{\mathrm{T}}\mathbf{w}_i\right|^2+\|\mathbf{u}_k\|^2\sigma^2}. \tag{25}$$

The CPU/reader performs the optimization by using the estimated CSI of the channels. Thus, channel coefficients in all objective functions and constraints in $\mathbf{P1}$ *are substituted with their respective channel estimations. Furthermore, the CPU/reader informs/controls the other nodes, i.e., APs and tags, via front-haul/back-haul links or control links [40], [41].*

The proposed sum rate maximization, $\mathbf{P1}$, has an objective function and constraints that are not convex functions in $\mathbf{w}_k$, $\mathbf{u}_k$, and α_k. Non-convex problems are hard to solve optimally. Such a problem may have multiple feasible regions and local optimal points within each region. The problem of finding the exact global solution to a non-convex problem is NP-hard. Therefore, we resort to decoupling the optimization variables and employ AO, FP, and Rayleigh ratio quotient approaches.

IV. Proposed Solution

As mentioned, the AO paradigm requires the optimization variables to be split into non-overlapping blocks of one or more block variables. This allows iterative optimization of one block variable at a time while holding the others fixed, then proceeds to optimize the next block while holding the others

fixed, and so on until convergence is attained. This method is also known as block coordinate descent [42]. In our problem, $\mathbf{w}_k$, $\mathbf{u}_k$, and α_k are the natural choice of blocks.

A. Transmit Beamforming

When the tags' reflection coefficients and the reader's receiver combining are fixed, $\mathbf{P1}$ reduces to the following transmit beamforming optimization problem:

$$\mathbf{P}_{\mathrm{w}}: \underset{\mathbf{w}_k \forall k}{\text{maximize}} \ \sum\nolimits_{k\in\mathcal{K}} \psi \log_2(1+\hat{\gamma}_k), \tag{26a}$$

$$\text{subject to} \ \sum\nolimits_{i\in\mathcal{K}} |w_{i,m}|^2 \le 1, \tag{26b}$$

$$(1-\alpha_k) p_t \left| \sum\nolimits_{i\in\mathcal{K}} \hat{\mathbf{f}}_k^{\mathrm{T}} \mathbf{w}_i \right|^2 \ge p_b', \tag{26c}$$

where $\hat{\gamma}_k$ is obtained by replacing the respective channels, i.e., $\mathbf{g}_k$ and $\mathbf{f}_k$ for $k \in \mathcal{K}$, in (25) with respective estimated channels.

Next, we define $\mathbf{a}_{kj} \triangleq [\mathbf{u}_k^{\mathrm{T}} \hat{\mathbf{g}}_j \hat{\mathbf{f}}_j^{\mathrm{T}}, \ldots, \mathbf{u}_k^{\mathrm{T}} \hat{\mathbf{g}}_j \hat{\mathbf{f}}_j^{\mathrm{T}}] \in \mathbb{C}^{MK\times 1}$ and $\mathbf{w} \triangleq [\mathbf{w}_1^{\mathrm{T}}, \ldots, \mathbf{w}_K^{\mathrm{T}}]^{\mathrm{T}} \in \mathbb{C}^{MK\times 1}$. Thereby, the T_k's SINR in (25) is rearranged as

$$\hat{\gamma}_k = \frac{\alpha_k p_t \left| \mathbf{a}_{kk}^{\mathrm{T}} \mathbf{w} \right|^2}{p_t \sum_{j\in\mathcal{K}_k} \alpha_j \left| \mathbf{a}_{kj}^{\mathrm{T}} \mathbf{w} \right|^2 + \sigma_w^2}, \tag{27}$$

where $\sigma_w^2 = \|\mathbf{u}_k\|^2 \sigma^2$. Then, $\mathbf{P}_{\mathrm{w}}$ can be treated as a multiple ratio FP problem [43], [44]. We next apply a quadratic transform to the objective function of $\mathbf{P}_{\mathrm{w}}$ as

$$f(\mathbf{w}, \boldsymbol{\lambda}) = \sum\nolimits_{k\in\mathcal{K}} \psi \log_2 \left(1 + 2\lambda_k \sqrt{\alpha_k p_t} \mathrm{Re}\left\{ \mathbf{a}_{kk}^{\mathrm{T}} \mathbf{w} \right\} - \lambda_k^2 \left(p_t \sum\nolimits_{j\in\mathcal{K}_k} \alpha_j |\mathbf{a}_{kj}^{\mathrm{T}} \mathbf{w}|^2 + \sigma_w^2 \right) \right), \tag{28}$$

where $\boldsymbol{\lambda} = [\lambda_1, \ldots, \lambda_K]^{\mathrm{T}}$ is the auxiliary variable introduced by the quadratic transformation. Thereby, we alternatively optimize $\mathbf{w}$ and $\boldsymbol{\lambda}$. For a given $\mathbf{w}$, the optimal $\boldsymbol{\lambda}$ is found in closed-form as [43]

$$\lambda_k^o = \frac{\sqrt{\alpha_k p_t} \mathrm{Re}\left\{ \mathbf{a}_{kk}^{\mathrm{T}} \mathbf{w} \right\}}{\ln(2) \left(p_t \sum_{j\in\mathcal{K}_k} \alpha_j |\mathbf{a}_{kj}^{\mathrm{T}} \mathbf{w}|^2 + \sigma_w^2 \right)}. \tag{29}$$

Remark 7. *Without losing generality, we constrain the transmit beamforming vector,* $\mathbf{w}$*, with the channel responses to obtain a non-negative real desired signal term, i.e.,* $\left| \mathbf{a}_{kk}^{\mathrm{T}} \mathbf{w} \right| \approx \mathrm{Re}\{\mathbf{a}_{kk}^{\mathrm{T}} \mathbf{w}\}$*. Our simulation findings support the validity of this technique. This is because our method iteratively maximizes the achievable rate/SINR by co-phasing the desired signal component while reducing interference.*

Next, we must optimize $\mathbf{w}$ for a given $\boldsymbol{\lambda}$. First, by applying several mathematical manipulations, the objective function in (28) can be rearranged as

$$f(\mathbf{w}) = \sum_{k\in\mathcal{K}} \psi \log_2 \left(1 - \mathbf{w}^{\mathrm{T}} \mathbf{U}_k \mathbf{w} + 2\mathrm{Re}\left\{ \mathbf{w}^{\mathrm{T}} \mathbf{v}_k \right\} + t_k \right), \tag{30}$$

where $\mathbf{U}_k$, $\mathbf{v}_k$, and t_k for $k \in \mathcal{K}$ are defined as

$$\mathbf{U}_k \triangleq (\lambda_k^o)^2 p_t \sum_{j\in\mathcal{K}_k} \alpha_j \mathbf{a}_{kk} \mathbf{a}_{kk}^{\mathrm{T}}, \tag{31a}$$

$$\mathbf{v}_k \triangleq 2\lambda_k^o \sqrt{\alpha_k p_t} \mathbf{a}_{kk}, \tag{31b}$$

$$t_k \triangleq (\lambda_k^o)^2 \sigma_w^2. \tag{31c}$$

Next, for a given $\boldsymbol{\lambda}$, the corresponding optimization problem is given as

$$\mathbf{P}_{\mathrm{w1}}: \underset{\mathbf{w}}{\text{maximize}} \ f(\mathbf{w}), \tag{32a}$$

$$\text{subject to} \ \sum\nolimits_{i\in\mathcal{K}} |w_{i,m}|^2 \le 1, \tag{32b}$$

$$(1-\alpha_k) p_t P_k^{\mathrm{Lin}} \ge p_b', \tag{32c}$$

where P_k^{Lin} is the linearized received signal power at T_k, and given as

$$P_k^{\mathrm{Lin}} = \left(\mathbf{w}^{(i-1)} \right)^{\mathrm{T}} \mathbf{D}_k \mathbf{w}^{(i-1)} + \left(\left(\mathbf{D}_k + \mathbf{D}_k^{\mathrm{T}} \right) \mathbf{w}^{(i-1)} \right)^{\mathrm{T}} \left(\mathbf{w}^{(i)} - \mathbf{w}^{(i-1)} \right), \tag{33}$$

where $\mathbf{D}_k = \mathbf{d}_k \mathbf{d}_k^{\mathrm{T}}$ and $\mathbf{d}_k \triangleq [\hat{\mathbf{f}}_k^{\mathrm{T}}, \ldots, \hat{\mathbf{f}}_k^{\mathrm{T}}]^{\mathrm{T}} \in \mathbb{C}^{MK\times 1}$. Besides, $\mathbf{w}^{(i)}$ and $\mathbf{w}^{(i-1)}$ are the current and the previous iteration values of $\mathbf{w}$.

Because $\mathbf{a}_{kj} \mathbf{a}_{kj}^{\mathrm{T}}$ is a positive-definite matrix, $\mathbf{U}_k$ is also a positive-definite matrix. Hence, the objective function, $f(\mathbf{w})$, is a quadratic concave function of $\mathbf{w}$. Consequently, $\mathbf{P}_{\mathrm{w1}}$ can be solved as a quadratically constrained quadratic program (QCQP) [45]. Conversely, it can be proved that for the optimal $\boldsymbol{\lambda}$, the solution to $\mathbf{P}_{\mathrm{w1}}$ also satisfies $\mathbf{P}_{\mathrm{w1}}$ (26) [43], [46]. Algorithm 1 gives the solution of $\mathbf{P}_{\mathrm{w1}}$.

Algorithm 1 : Transmit beamforming.

Initialization: Initialize $\mathbf{w}$ to a feasible value.
Repeat
Step 1: Update λ by (29).
Step 2: Update $\mathbf{w}$ by solving $\mathbf{P}_{\mathrm{w1}}$ in (32).
Until the value of the objective function converges.
Output: The optimal transmit beamforming vector $\mathbf{w}^o$.

Remark 8. *The proposed optimization strategy for solving* $\mathbf{w}$ *once the original problem,* $\mathbf{P}_{\mathrm{w}}$*, is transformed into a convex problem is shown in Algorithm 1. An alternating optimization strategy is used to solve* $\mathbf{P}_{\mathrm{w}}$ *iteratively. We begin by quantifying the SINR in* (25) *upon initializing* $\mathbf{w}$*, and then we update a better solution for* $\mathbf{w}$ *in each iteration. This process is repeated until the normalized objective function increases less than* $\epsilon = 10^{-3}$*.*

B. Receiver Combining

Here, we design the reader's combining filters. To this end, for fixed transmit beamforming and tags' reflection coefficients, $\mathbf{P1}$ is reduced to a receiver combining optimization problem and is formulated as

$$\mathbf{P}_{\mathrm{u}}: \underset{\mathbf{u}_k, \forall k}{\text{maximize}} \ \sum\nolimits_{k\in\mathcal{K}} \psi \log_2(1+\hat{\gamma}_k), \tag{34a}$$

$$\text{subject to} \ \|\mathbf{u}_k\|^2 \le 1. \tag{34b}$$

We first define $\mathbf{b}_k \triangleq \mathbf{g}_k \sum_{i\in\mathcal{K}} \mathbf{f}_k^{\mathrm{T}}\mathbf{w}_i$ and rewrite the T_k's SINR in (25) as

$$\begin{aligned}\hat{\gamma}_k &= \frac{\alpha_k p_t \left|\mathbf{b}_k^{\mathrm{T}}\mathbf{u}_k\right|^2}{p_t \sum_{j\in\mathcal{K}_k} \alpha_j \left|\mathbf{b}_j^{\mathrm{T}}\mathbf{u}_k\right|^2 + \|\mathbf{u}_k\|^2\sigma^2} \\ &= \frac{\mathbf{u}_k^{\mathrm{T}}\mathbf{B}_k\mathbf{u}_k}{\mathbf{u}_k^{\mathrm{T}}\left(\sum_{j\in\mathcal{K}_k}\mathbf{B}_j + \sigma^2\mathbf{I}_L\right)\mathbf{u}_k},\end{aligned} \tag{35}$$

where $\mathbf{B}_j = \alpha_j p_t \mathbf{b}_j\mathbf{b}_j^{\mathrm{T}}$. Since the objective function in (34a) is a non-decreasing function of its argument, it can be replaced by the SINR of T_k (35), i.e., $\sum_{k\in\mathcal{K}}\log_2(1+\hat{\gamma}_k) = \sum_{k\in\mathcal{K}}\hat{\gamma}_k$. $\mathbf{P}_{\mathrm{u}}$ thus becomes a generalized Rayleigh ratio quotient problem [47], [48]. Hence, the optimal combiner vector for T_k is given as [47], [48]

$$\mathbf{u}_k^o = v_{\max}\left[\left(\sum_{j\in\mathcal{K}_k}\mathbf{B}_j + \sigma^2\mathbf{I}_L\right)^{-1}\mathbf{B}_k\right], \tag{36}$$

where $v_{\max}[\cdot]$ is the dominant eigenvector of the matrix [47], [48].

C. Reflection Coefficient Optimization

As the final block of the proposed AO framework, we optimize the tags' reflection coefficients here. For given transmit beamforming and receiver combining, $\mathbf{P1}$ becomes an optimization problem for tags' reflection coefficients. The corresponding optimization problem is given as

$$\mathbf{P}_\alpha : \underset{\alpha_k,\forall k}{\text{maximize}} \ \sum\nolimits_{k\in\mathcal{K}} \psi\log_2(1+\hat{\gamma}_k), \tag{37a}$$

$$\text{subject to} \ \ (1-\alpha_k)p_t\left|\sum\nolimits_{i\in\mathcal{K}}\mathbf{f}_k^{\mathrm{T}}\mathbf{w}_i\right|^2 \geq p_b', \tag{37b}$$

$$0<\alpha_k<1. \tag{37c}$$

To solve $\mathbf{P}_\alpha$, we first introduce θ_k to replace the SINR terms in (37a), such that $\theta_k \leq \hat{\gamma}_k$, and then reformulate $\mathbf{P}_\alpha$ as follows:

$$\mathbf{P}_{\alpha1} : \underset{\boldsymbol{\alpha},\boldsymbol{\theta}}{\text{maximize}} \ \sum\nolimits_{k\in\mathcal{K}} \psi\log_2(1+\theta_k), \tag{38a}$$

$$\text{subject to} \ \ \theta_k \leq \frac{\hat{A}_k(\boldsymbol{\alpha})}{\hat{B}_k(\boldsymbol{\alpha})}, \tag{38b}$$

$$(1-\alpha_k)p_t\left|\mathbf{d}_k^{\mathrm{T}}\mathbf{w}\right|^2 \geq p_b', \tag{38c}$$

$$0<\alpha_k<1, \tag{38d}$$

where $\boldsymbol{\alpha} = [\alpha_1,\ldots,\alpha_K]^{\mathrm{T}}$ and $\boldsymbol{\theta} = [\theta_1,\ldots,\theta_K]^{\mathrm{T}}$. Besides, $\hat{A}_k(x)$ and $\hat{B}_k(x)$ are the numerators and denominators of the corresponding SINR terms $\hat{\gamma}_k$ as functions of the variable x i.e., $\boldsymbol{\alpha}$. The reformulated optimization problem $\mathbf{P}_{\alpha1}$ can be considered as a two-part optimization problem, i.e., (i) an outer optimization over $\boldsymbol{\alpha}$ with fixed $\boldsymbol{\theta}$ and (ii) an inner optimization over $\boldsymbol{\theta}$ with fixed $\boldsymbol{\alpha}$.

The inner optimization problem is thus given as

$$\mathbf{P}_{\alpha2} : \underset{\boldsymbol{\alpha},\boldsymbol{\theta}}{\text{maximize}} \ \sum\nolimits_{k\in\mathcal{K}} \psi\log_2(1+\theta_k), \tag{39a}$$

$$\text{subject to} \ \ \theta_k \leq \frac{\hat{A}_k(\boldsymbol{\alpha})}{\hat{B}_k(\boldsymbol{\alpha})}. \tag{39b}$$

This inner optimization problem in (39) is convex in $\boldsymbol{\theta}$ and has strong duality [43]. Thus, he solution to $\mathbf{P}_{\alpha2}$ is that θ_k satisfies (39b) with equality. We use the Lagrangian dual transform [43] to deal with the logarithm in the objective function of $\mathbf{P}_{\alpha2}$, and the corresponding Lagrangian function is given as

$$L(\boldsymbol{\theta},\boldsymbol{\mu}) = \sum_{k\in\mathcal{K}}\psi\log_2(1+\theta_k) - \sum_{k\in\mathcal{K}}\mu_k\left(\theta_k - \frac{\hat{A}_k(\boldsymbol{\alpha})}{\hat{B}_k(\boldsymbol{\alpha})}\right), \tag{40}$$

where $\boldsymbol{\mu} = [\lambda_1,\ldots,\lambda_K]^{\mathrm{T}}$ is the dual variable vector introduced for each inequality constraint in (39b). From the strong duality, $\mathbf{P}_{\alpha2}$ is equivalently reformulated to a dual problem as follows:

$$\mathbf{P}_{\alpha3} : \underset{\boldsymbol{\mu}\succeq0}{\text{minimize}} \quad \underset{\boldsymbol{\theta}}{\text{maximize}} \quad L(\boldsymbol{\theta},\boldsymbol{\mu}). \tag{41}$$

The optimal solution of μ_k can then be obtained by evaluating the first-order condition $\partial L(\boldsymbol{\theta},\boldsymbol{\mu})/\partial\theta_k$ and applying the trivial solution to $\mathbf{P}_{\alpha2}$ as

$$\mu_k^o = \frac{\psi\hat{B}_k(\boldsymbol{\alpha})}{\hat{A}_k(\boldsymbol{\alpha}) + \hat{B}_k(\boldsymbol{\alpha})}. \tag{42}$$

Besides, $\mu_k \geq 0$ is automatically satisfied. Using (40) and (42), $\mathbf{P}_{\alpha2}$ is reformulated as

$$\mathbf{P}_{\alpha4} : \underset{\boldsymbol{\theta}}{\text{maximize}} \quad L(\boldsymbol{\theta},\boldsymbol{\mu}^o). \tag{43}$$

Further, it can be shown the solution to $\mathbf{P}_{\alpha4}$ satisfies $\mathbf{P}_\alpha$ when combined with the outer optimization over $\boldsymbol{\alpha}$ and after several mathematical interpretations [43], [49]. Thus, the tag reflection coefficients, $\boldsymbol{\alpha}$, are obtained by solving feasibility problem over $\boldsymbol{\alpha}$ for fixed $\boldsymbol{\theta}$. The corresponding optimization problem is thus given as

$$\mathbf{P}_{\alpha5} : \text{find} \ \ \boldsymbol{\alpha}, \tag{44a}$$

$$\text{subject to} \ \ \theta_k^o \leq \frac{\hat{A}_k(\boldsymbol{\alpha})}{\hat{B}_k(\boldsymbol{\alpha})}, \tag{44b}$$

$$(1-\alpha_k)p_t\left|\mathbf{d}_k^{\mathrm{T}}\mathbf{w}\right|^2 \geq p_b', \tag{44c}$$

$$0<\alpha_k<1. \tag{44d}$$

Algorithm 2 provides the proposed approach for optimizing the tags' reflection coefficients.

Algorithm 2 : Reflection coefficient optimization.

Initialization: Initialize $\boldsymbol{\alpha}$ to a feasible value.
Repeat
Step 1: Update $\boldsymbol{\mu}$ by (42).
Step 2: Update $\boldsymbol{\theta}$ by solving $\mathbf{P}_{\alpha4}$ in (43).
Step 3: Update $\boldsymbol{\alpha}$ by solving $\mathbf{P}_{\alpha5}$ in (44).
Until the value of the objective function converges.
Output: The optimal reflection coefficients $\boldsymbol{\alpha}^o$.

Remark 9. *Algorithm 3 presents the overall algorithm for solving the proposed optimization problem,* $\mathbf{P1}$ (23)*. We begin by setting* $\mathbf{u}_k$ *for* $k\in\mathcal{K}$ *and* $\boldsymbol{\alpha}$ *to random feasible values. Then, in each iteration, algorithms update better solutions for* $\mathbf{w}$*,* $\mathbf{u}_k$*, and* $\boldsymbol{\alpha}$ *until the objective function no longer improves. The procedure is terminated when the normalized objective function increment is less than* $\epsilon = 10^{-3}$*.*

It is important to note that the initialization of variables significantly influences the algorithm's convergence. Rapid

Algorithm 3 : Overall algorithm.

Initialization: Initialize $\mathbf{u}_k$ for $k \in \mathcal{K}$ and $\boldsymbol{\alpha}$ to a feasible values.
Repeat
Step 1: Update $\mathbf{w}$ by solving $\mathbf{P}_{\mathrm{w}}$ in (26).
Step 2: Update $\mathbf{u}_k$ for $k \in \mathcal{K}$ by solving $\mathbf{P}_{\mathrm{u}}$ in (34).
Step 3: Update $\boldsymbol{\alpha}$ by solving $\mathbf{P}_{\alpha}$ in (37).
Until the value of the objective function converges.
Output: The optimal beamforming $\mathbf{w}^o$, receiver combining $\mathbf{u}_k^o$, and reflection coefficients $\boldsymbol{\alpha}^o$.

convergence is achieved when the initial value is closer to the optimal value. However, determining a near-optimal initial guess for a complex optimization problem with constraints is challenging and escalates overall computational complexity [45]. As a result, adopting random feasible initial values is a standard practice [43], [50], and we adhere to this approach. Furthermore, simulation results demonstrate that our overall and individual algorithms exhibit rapid convergence irrespective of the random initial values.

Remark 10. *In $\mathbf{P}_{\mathrm{w}}$ and $\mathbf{P}_{\alpha}$, we employ the FP for obtaining transmit beamformers. As a well-established optimization method, the FP transforms the original multi-ratio problem into an equivalent problem by decoupling the numerators and denominators using the quadratic transformation [43], [46], [51]. Thus, the FP preserves the original problem and does not result in performance losses. However, as the Taylor series linearization technique is used for the EH constraint in $\mathbf{P}_{\mathrm{w}}$, it may introduce some performance losses.*

In contrast, the Rayleigh ratio quotient approach in $\mathbf{P}_{\mathrm{u}}$ yields the closed-form optimal solution. There is no equivalent transformation or conversion for this sub-problem, hence there is no performance loss [47], [48].

D. Optimality

Depending on the optimalities of the underlying sub-problems, the AO can generate a globally or locally optimal solution. Generally, if each underlying sub-problem separately yields globally optimal solutions, the overall AO algorithm achieves global optimality. Otherwise, it offers a locally optimal solution [52]. In the proposed AO algorithm, two of the sub-problems, i.e., $\mathbf{P}_{\mathrm{w}}$ and $\mathbf{P}_{\alpha}$, are solved utilizing FP approaches, while the remaining sub-problem, i.e., $\mathbf{P}_{\mathrm{u}}$, is addressed with the Rayleigh ratio quotient approach.

As the Rayleigh ratio quotient approach yields a closed-form solution, it ensures the global optimal solution for $\mathbf{P}_{\mathrm{u}}$ [47], [48]. In contrast, the FP guarantees global optimality for single-ratio problems. However, for multi-ratio cases, it generally offers a locally optimal solution [43], [46], [51]. Since $\mathbf{P}_{\mathrm{w}}$ and $\mathbf{P}_{\alpha}$ are multi-ratio problems, their solutions are sub-optimal, i.e., locally optimal. As a result, the suggested AO algorithm typically achieves a locally optimal solution.

E. Computational Complexity

The proposed AO solution is a multi-stage iterative algorithm. Here, the outer loop has three sub-problems for optimizing $\mathbf{w}$, $\mathbf{u}_k$ for $k \in \mathcal{K}$, and $\boldsymbol{\alpha}$. Each sub-problem requires an iterative updating method to solve. Specifically, the computational complexity of Algorithm 1 lies in Step 2. Matlab CVX uses the SDPT3 solver for solving the sub-problem for $\mathbf{w}$. Thus, the computational complexities of Algorithm Algorithm 1 is $\mathcal{O}(M^3K^3)$ [51], [53]. The computational complexity of the sub-problem for solving $\mathbf{u}_k$ for $k \in \mathcal{K}$ is in the matrix inversion, multiplication, and eigenvalue decomposition (36). Hence, the computational complexity is $\mathcal{O}(K^3(2K^2+1))$. The computational complexity of Algorithm 2 lies in step 3. Similar to Algorithm 1, CVX Matlab uses an SDPT3 solver to handle this optimization problem. Therefore, the computational complexity of Algorithm 2 is $\mathcal{O}(M^3K^3)$ [51], [53]. Hence, the total complexity of the proposed AO solution is $\mathcal{O}(I_o(I_wM^3K^3 + K^3(2K^2 + 1) + I_\alpha M^3K^3))$, where I_w, I_α, and I_o are the iteration numbers of Algorithm 1, Algorithm 2, and the overall algorithm (outer loop – Algorithm 3), respectively [51], [53].

F. Algorithm Convergence

Generally, an AO algorithm for a maximization problem converges to global or local maximizers [52, Theorem 2]. This methodology exhibits exceptional efficiency for problems where a clear partitioning of variables exists, allowing for explicit (closed-form) partial maximizers within some or all sub-problems.

In our AO solution, we utilize the FP technique to solve $\mathbf{w}$ and $\boldsymbol{\alpha}$ blocks, whereas $\mathbf{u}_k$ for $k \in \mathcal{K}$ is obtained as a closed-form solution applying the Rayleigh ratio quotient approach. Hence, overall algorithm convergence relies on the FP. Interestingly, the FP yields a fixed-point iteration method with provable convergence [43], [46], [51], ensuring the convergence of our proposed AO method. Nonetheless, our simulation results also corroborate the validity of this claim (Fig. 6).

Conversely, the convergences of individual algorithms (i.e., Algorithm 1 and Algorithm 2) directly affect the overall algorithm (i.e., Algorithm 3) convergence and hence, the execution time. However, the main challenge is the non-convex nature of the optimization problem. Thus, many existing works on both conventional communication and BackCom take the same AO approach to tackle non-convex problems, assuming the execution time is much lower than the coherence interval [19], [27], [44], [49]. In this work, we implement the solution based on the same assumption.

V. Simulation Results

Herein, we present simulation examples for evaluating the performance of the proposed cell-free BiBC system.

We adopt a three-slope model for modeling the large-scale fading ζ_v (1) with operating frequency, f_c, in MHz [40]. In particular, for reference distances $d_0 = 10\,\mathrm{m}$ and $d_1 = 50\,\mathrm{m}$, the path loss exponent is (i) 3.5 if the distance between two nodes in m (denoted by d) is larger than d_1, (ii) 2 if $d_1 \geq d > d_0$, and (iii) 0 if $d \leq d_0$. When $d > d_1$, the Hata-COST231

TABLE II: Simulation settings.

Parameter	Value	Parameter	Value
f_c	2 GHz	M	36
B	10 MHz	L	4
N_f	10 dB	K	{3, 5}
d_0, d_1	{10, 50}m	p_b	−20 dBm
h_{AP}, h_T, h_R	{15, 1, 1.6}m	p_p	20 dBm
τ_c	1000	τ	5

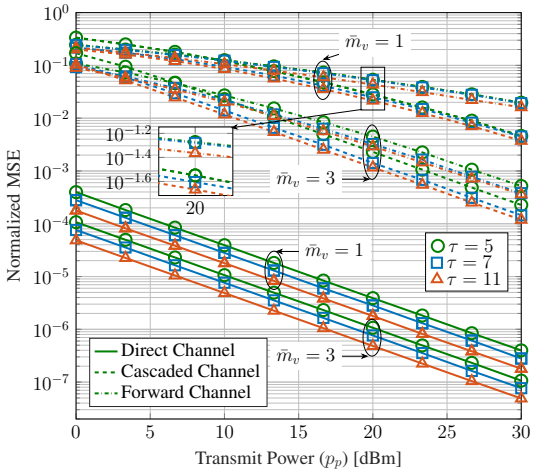

Fig. 4: Normalized MSE of direct, cascaded, and forward channels for $K = 3$, $\bar{m}_v = \{1, 3\}$, and $\tau = \{5, 7, 11\}$.

propagation model is employed. The path loss in dB is then defined as

$$\zeta_v = \begin{cases} -L - 35\log_{10}(d), & \text{if } d > d_1, \\ -L - 15\log_{10}(d_1) - 20\log_{10}(d), & \text{if } d_0 < d \le d_1, \\ -L - 15\log_{10}(d_1) - 20\log_{10}(d_0), & \text{if } d \le d_0, \end{cases} \quad (45)$$

where $L = 46.3 + 33.9\log_{10}(f_c) - 13.82\log_{10}(h_t) - (1.1\log_{10}(f_c) - 0.7)h_r + (1.56\log_{10}(f_c) - 0.8)$. Here, h_t and h_r denote the transmitter and receiver antenna heights in m, respectively, i.e., AP antenna height, h_{AP}, tag antenna height, h_T, and reader antenna height, h_R. The AWGN variance, σ^2 is modeled as $\sigma^2 = 10\log_{10}(N_0 B N_f)$ dBm, where $N_0 = -174$ dBm/Hz, B is the bandwidth, and N_f is the noise figure.

To model the coverage area, e.g., warehouse, we consider a $50 \times 50\,\mathrm{m}^2$ square area, the reader is located at the center, the APs are uniformly distributed, and the tags are randomly distributed within the area. Unless otherwise specified, Table II gives the simulation parameters.

A. Channel Estimation

We first investigate the performance of our channel estimation method (section II-D), considering the LS estimator. Note that the MVU estimator matches the LS estimator in the simulation (Remark 3).

The quality of the channel estimator is assessed in terms of normalized MSE, which is defined as

$$\text{Normalized MSE} = \frac{\mathbb{E}\left\{\|\mathbf{v} - \hat{\mathbf{v}}\|^2\right\}}{\mathbb{E}\left\{\|\mathbf{v}\|^2\right\}}, \quad (46)$$

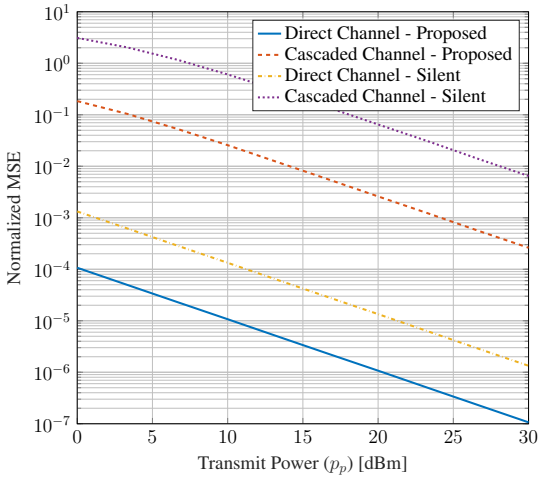

Fig. 5: Normalized MSE of direct and cascaded channels for $K = 3$, $\bar{m}_v = 3$, and $\tau = 5$.

where $\mathbf{v} \in \{\mathbf{h}_{0,m}, \mathbf{h}_{k,m}, f_{k,m}\}$.

Fig. 4 shows the normalized MSE (NMSE) performance of the LS estimator versus the per-AP pilot transmit power p_p for the direct, cascaded, and forward channels, considering $K = 3$, $\bar{m}_v = \{1, 3\}$, and $\tau = \{5, 7, 11\}$. Our method demonstrates high estimation accuracy for all the channels for multiple tag scenarios. However, the NMSE for the cascaded and the forward channels is compared to that for the direct channel. This is primarily due to the double path loss in the cascaded and the forward channels and the tag's reflection coefficient α. We also observe that increasing the pilot sequence length improves the estimation accuracy and lowers the required transmit power for a given MSE level. For instance, for the direct link, an NMSE of 10^{-5} is achieved at 12 dBm and 16 dBm for $\tau = 11$ and $\tau = 5$, respectively. Similarly, increasing the pilot length from $\tau = 5$ and $\tau = 11$ can save 2.5 dBm dB and 2 dBm of transmit power, respectively, to obtain an NMSE of 2×10^{-2} in the forward channel and 5×10^{-3} in the cascaded channel. Furthermore, the NMSE trend scales with the fading model's severity, i.e., low NMSEs for large $\bar{m}_v$ values.

Conversely, Fig. 5 depicts the NMSE of the direct and cascaded channels for the proposed channel estimation scheme and the commonly used 'silent protocol'-based channel estimation method [11]. Fig. 5 plots the NMSE as a function of per-AP pilot transmit power, p_p, for $K = 3$, $\tau + 5$, and $\bar{m}_v = 3$. Our proposed method remarkably outperforms the silent protocol regarding channel estimation accuracy for both direct and cascade channels. The main reason for this significant performance improvement is that our method utilizes the entire pilot length while preventing pilot contamination. In contrast, the silent case uses only a portion of the pilot sequence for each channel estimation [15].

Note that using the highly accurate estimates of the direct link channels, the reader can cancel out the direct link interference, thereby justifying the assumption stated in Remark 4.

In the following, we use these channel estimates to evaluate the performance of our proposed schemes for the BiBC

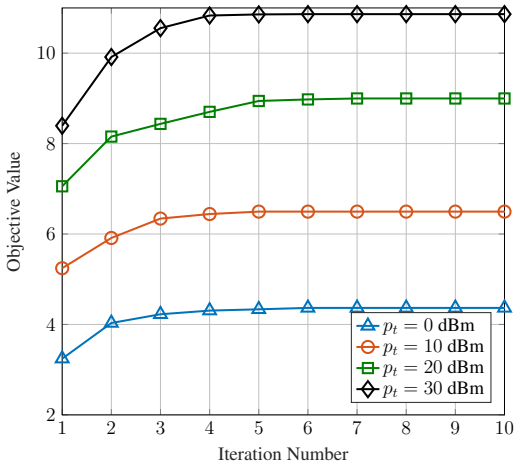

Fig. 6: The convergence of the objective value of the overall algorithm.

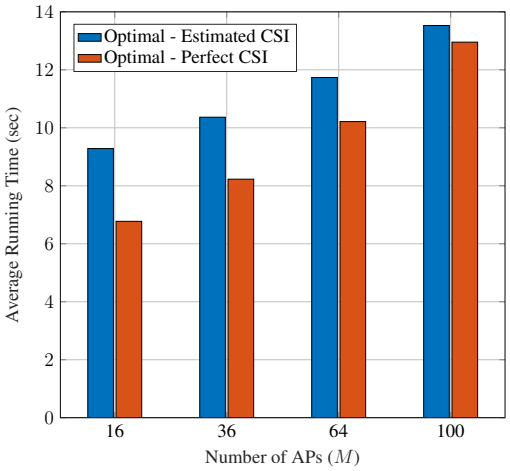

Fig. 7: The overall algorithm running time versus the number of APs for $K = 3$ and $p_t = 20\,\mathrm{dBm}$.

network, for $p_p = 20\,\mathrm{dBm}$ and $\tau = 5$. Moreover, unless otherwise specified, the Nakagami-m parameter, $\bar{m}_v$, is set to 1.

B. Convergence Rate of the Proposed Algorithm

Before proceeding to the performance analysis, we investigate the convergence rate of the proposed algorithm (Section IV, Remark 9). To this end, Fig. 6 shows its convergence behavior for when the AP is at $p_t = \{0, 10, 20, 30\}$ dBm. The objective function of the overall algorithm is the sum rate. The stopping condition for convergence is that the increment of the normalized objective function is less than $\epsilon = 10^{-3}$. As shown in Fig. 6, the sum rate achieved by the overall Algorithm 3 increases rapidly and saturates as the number of iterations increases. Specifically, it converges in less than five iterations regardless of the AP transmit power.

C. Algorithm Execution Time

Fig. 7 shows the correlation between the execution time and the number of APs, M for $K = 3$ and $p_t = 20\,\mathrm{dBm}$. These data are from Matlab simulations from an Intel® Core™ i7 processor, clocking at $2.8\,\mathrm{GHz}$. As per Fig. 7, the overall algorithm execution time for all schemes is directly proportional to M, i.e., running time (or computational demand) grows as M increases. This trend reveals the complicated challenges of dealing with more APs, emphasizing the importance of efficient algorithms. Compared to the perfect CSI case, the estimated CSI scheme has a slightly high computational time. The main explanation is that the algorithm consumes additional time for estimating the channels and dealing with channel estimation errors. However, with a high number of APs, the average running time gap between perfect CSI and estimated CSI narrows. This is because the total transmit power of the system increases with the number of APs, resulting in more accurate channel estimates and smaller estimation errors.

This study primarily examines application scenarios in environments such as warehouses and agriculture, where low-mobility devices or tags are deployed, constituting emerging backscatter networks as defined in the 3GPP standard [1]–[3]. The channels exhibit long coherence times in these settings due to the low mobility [1]–[3]. Furthermore, the execution time of the algorithm is primarily contingent upon the hardware and computational capacity of the reader or CPU, which typically includes dedicated computational hardware. Consequently, the runtime is expected to be significantly shorter than the illustration in Fig. 7 and will likely be well below the coherence time.

D. Performance Analysis

In this section, we assess the performance of the proposed cell-free BiBC network. We evaluate the ability of proposed power allocation and channel estimation schemes to enhance the received power at the tags and the sum rate. We consider two comparative benchmarks:

- A_1 *Random beamforming*: Optimal beamforming hinges on the availability of perfect CSI. Random beamforming emerges as a viable alternative when perfect CSI is inaccessible. Asymptotically, the performance of random beamforming is not bad. For example, with M transmit antennas and n users, both optimal and random beamforming exhibit the same asymptotic sum-rate capacity of $M \log(n)$, as established by [54], [55]. This intriguing observation validates the adoption of random beamforming when CSI is unattainable. To implement this approach, we opt for complex Gaussian random vectors for $\mathbf{w}$ and $\mathbf{u}_k, (k \in \mathcal{K})$, ensuring adherence to the per-AP transmit power constraint (23b) and the reader's normalized power constraint (23d). The tag reflection coefficients are set to 0.6.
- A_2 *Optimal beamforming with perfect CSI*: $\mathbf{w}$, $\mathbf{u}_k\,(k \in \mathcal{K})$, and $\boldsymbol{\alpha}$ are obtained through the proposed optimization framework with perfect CSI, i.e., without performing channel estimation.
- A_3 *Optimal beamforming with estimated CSI*: $\mathbf{w}$, $\mathbf{u}_k\,(k \in \mathcal{K})$, and $\boldsymbol{\alpha}$ are obtained using the proposed optimization

framework with estimated CSI using the proposed channel estimation.

1) Received Power at the Tag: Increasing this quantity is critical to ensure that the tag can be activated.

To see if our solution achieves this objective, we plot Fig. 8 and Fig. 9 of the received power by a tag, delineated for variations in transmit power and the number of APs. Notably, these figures also incorporate the activation threshold, $p_b = -20\,\mathrm{dBm}$, a reference point derived from commercial RFID tags [7], thereby providing invaluable insights into our analysis. Examining Fig. 8 and Fig. 9 underscores the efficacy of our proposed channel estimation and optimization frameworks. Our solution consistently delivers higher power to the tags across various transmit power settings and AP quantities. Other solutions such as random beamforming (A_1) necessitate escalated transmit power levels and an increased number of APs to attain the power threshold requisite for the tags. For instance, the A_1 approach mandates a minimum of $12\,\mathrm{dBm}$ when paired with 36 APs (Fig. 8), or 12 APs at $20\,\mathrm{dBm}$ (Fig. 9) to exceed the activation threshold. Evidently, from an energy efficiency perspective, random beamforming is sub-optimal. Our proposed algorithms bring much-needed energy savings.

However, it is important to note that while effective, our proposed channel estimation scheme falls short of the ideal performance achieved by perfect CSI benchmark A_2. Despite this disparity, there are strategic measures to bridge the gap:

1) **Allocating higher transmit power at APs:** Boosting the AP power enhances the SNR and mitigates the impact of imperfect channel estimation.
2) **Deploying more APs:** Denser AP deployments can increase diversity and redundancy, mitigating potential performance gaps.
3) **Employing longer pilot sequences:** This offers finer granularity in channel estimation, allowing for improved accuracy even with non-ideal schemes.

While our proposed CSI estimation method is imperfect, it can harmoniously integrate with these complementary solutions to attain remarkably high-performance standards.

2) Achievable Sum Rate: The achievable sum rate of the tags is investigated in Fig. 10 and Fig. 11, for different numbers of tags $K = \{3, 5\}$.

Fig. 10 illustrates the sum rate achieved by the tags as a function of the transmit power, p_t. It reveals that random beamforming designs, which do not use CSI, attain the lowest sum rate as they shape the beam in arbitrary directions. In contrast, our optimal beamforming designs achieve significant sum rates under both perfect and estimated CSI. Additionally, the achieved sum rate using the estimated CSI is comparable to that achieved with perfect CSI, demonstrating the efficiency of our channel estimation strategy. In particular, the optimal designs under perfect and estimated CSI improve the achieved sum rate respectively $425\,\%$ and $375\,\%$ compared to the random designs for $K = 5$, and $p_t = 10\,\mathrm{dBm}$.

Fig. 11 also depicts the achieved sum rate versus the number of APs for $p_t = 20\,\mathrm{dBm}$, and $K = \{3, 5\}$. Unlike random designs, the achieved sum rate significantly improves through optimal beamforming designs due to the efficient use of resources. These findings reveal the effectiveness of our proposed resource allocation and CSI estimation frameworks.

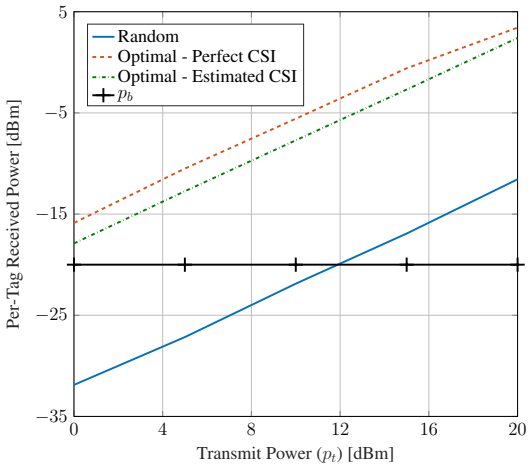

Fig. 8: Per-tag received power versus the transmit power.

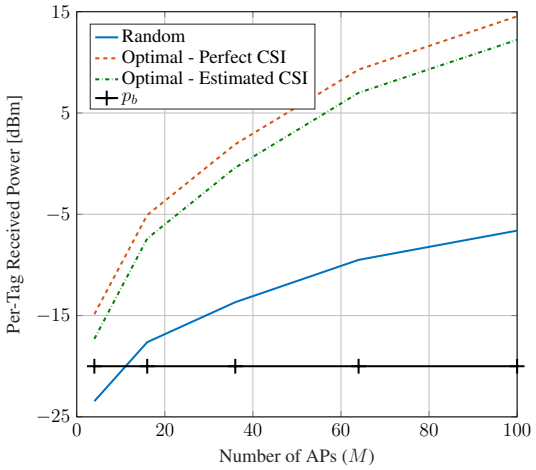

Fig. 9: Per-tag received power versus the number of APs for $p_t = 20\,\mathrm{dBm}$.

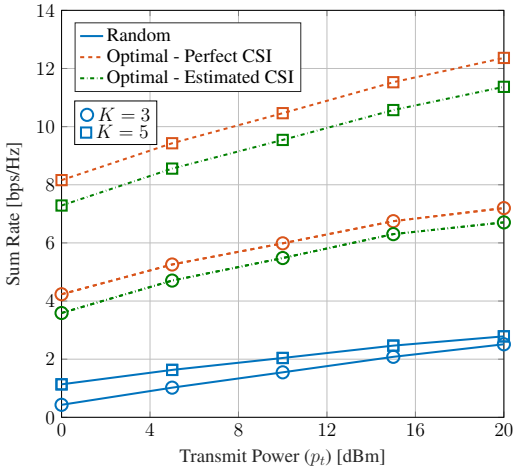

Fig. 10: Sum rate versus the transmit power.

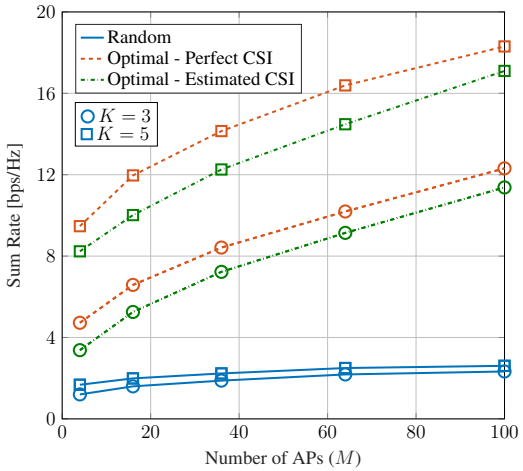

Fig. 11: Sum rate versus the number of APs for $p_t = 20\,\mathrm{dBm}$.

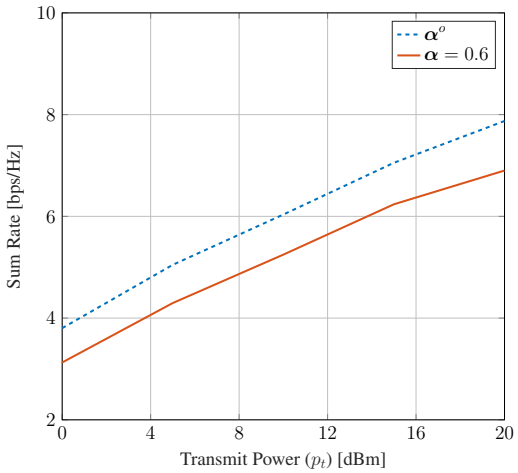

Fig. 12: Sum rate versus the transmit power for $K = 3$.

3) Fixed or Reconfigurable $\boldsymbol{\alpha}$: How much performance gains are possible by going from fixed to variable tags? To answer this question, we compare the performances of these two types of tags. Thus, we evaluate fixed tags ($\alpha_k = 0.6$ for $k \in \mathcal{K}$) using the proposed beamforming at APs and combining at the reader. We thus plot the achieved rates of the sum rate as a function of the AP transmit power in Fig. 12. As expected, the sum rate significantly improves when the tags use optimal $\boldsymbol{\alpha}^o$. For example, optimal $\boldsymbol{\alpha}^o$ achieves $\sim$1 bps/Hz at $p_t = 20\,\mathrm{dBm}$ than that of the tags with fixed $\boldsymbol{\alpha}$. Furthermore, depending on the application requirements and environment, our optimization framework is flexible enough to handle either tags with fixed α or tags with variable α.

VI. Conclusion

We investigated how to ensure robust energy harvests for tags within a large BiBC network. The problem is that some tags receive weak RF signals for EH in large areas such as warehouses. Our proposed solution introduces a cell-free, distributed access AP-assisted BiBC configuration, which enhances EH reliability across multiple tags and reduces their performance reliance on spatial positioning.

To achieve this objective, we introduced a channel estimation scheme tailored to accommodate the passive transmission characteristics of tags. We leveraged these channel estimates to determine optimal beamforming weights at the APs, reflection coefficients at the tags, and combining vectors at the reader. We aimed to maximize the aggregate tag data rate while satisfying the minimum energy requirements.

Notably, the optimization problems posed by these intricate scenarios are inherently non-convex. We developed a solution based on AO, FP, and Rayleigh Ratio Quotient approaches to address this challenge.

While our study was primarily developed with reconfigurable backscatter tags in mind, it can also work for tags with fixed reflection coefficients. The latter option, characterized by its cost-effectiveness and simplicity, presents a viable networking alternative. Conversely, while more costly, reconfigurable tags possess the potential to enhance overall network performance significantly.

Our research lays the groundwork for the evolution of cell-free BiBC systems equipped to accommodate multiple tags, bolstering their readiness to support emerging IoT networks.

Appendix A
Derivation of MMSE Estimator in (6)

We first evaluate the expectation term in the numerator as

$$\begin{aligned}\mathbb{E}\{h_{l,k}^m (y_{l,k}^m)^*\} &= \mathbb{E}\{h_{l,k}^m (\sqrt{p_p}(h_{l,k}^m)^* + (n_{l,k}^m)^*)\} \\ &= \sqrt{p_p}\mathbb{E}\{h_{l,k}^m (h_{l,k}^m)^*\} + \mathbb{E}\{h_{l,k}^m (n_{l,k}^m)^*\} \\ &= \begin{cases} \sqrt{p_p}\beta_{h_{0,lm}}, & \text{for} \quad k = 0, \\ \sqrt{\alpha_k p_p}\beta_{h_{k,lm}}, & \text{for} \quad k \in \mathcal{K}, \end{cases} \end{aligned} \tag{47}$$

where β_{mk} is given in (7). Next, the expectation term in the denominator is obtained as

$$\begin{aligned}\mathbb{E}\{|y_{l,k}^m|^2\} &= p_p \mathbb{E}\{|h_{l,k}^m|^2\} + \mathbb{E}\{|n_{l,k}^m|^2\} \\ &= \begin{cases} p_p \beta_{h_{0,lm}} + \sigma_p^2, & \text{for} \quad k = 0, \\ \alpha_k p_p \beta_{h_{k,lm}} + \sigma_p^2, & \text{for} \quad k \in \mathcal{K}. \end{cases} \end{aligned} \tag{48}$$

Hence, the MMSE of $h_{l,k}^m$ is given as (6).

References

[1] "3GPP TSG RAN −94e, Moderator's summary for discussion [RAN94e-R18Prep-28] passive IoT (from RP-212688)," Dec. 2021. Available Online: https://portal.3gpp.org/ngppapp/TdocList.aspx?meetingId=60043.

[2] "3GPP TSG RAN −97e3, Study on ambient IoT , 9.1 (from RP-222685)," Sept. 2022. Available Online: https://portal.3gpp.org/ngppapp/TdocList.aspx?meetingId=60043.

[3] "3GPP TSG RAN Meeting −94e, Study proposal on passive IoT, 8A.1 (from RP-213368)," Dec. 2021. Available Online: https://www.3gpp.org/DynaReport/TDocExMtg--RP-94-e--60214.htm.

[4] D. Galappaththige, F. Rezaei, C. Tellambura, and S. Herath, "Link budget analysis for backscatter-based passive IoT," *IEEE Access*, vol. 10, pp. 128890–128922, Dec. 2022.

[5] F. Rezaei, D. Galappaththige, C. Tellambura, and S. Herath, "Coding techniques for backscatter communications - A contemporary survey," *IEEE Commun. Surveys Tuts.*, pp. 1–1, 2th Quat. 2023.

[6] D. T. Hoang, D. Niyato, D. I. Kim, N. V. Huynh, and S. Gong, *Ambient Backscatter Communication Networks*. Cambridge University Press, 2020.

[7] RFID Tags, "GAO RFID Inc.," Available Online: https://gaorfid.com/.

[8] H. Q. Ngo, L. Tran, T. Q. Duong, M. Matthaiou, and E. G. Larsson, "On the total energy efficiency of cell-free massive MIMO," *IEEE Trans. Green Commun. Netw.*, vol. 2, pp. 25–39, Mar. 2018.

[9] E. Nayebi, A. Ashikhmin, T. L. Marzetta, H. Yang, and B. D. Rao, "Precoding and power optimization in cell-free massive MIMO systems," *IEEE Trans. Wireless Commun.*, vol. 16, pp. 4445–4459, Jul. 2017.

[10] D. Galappaththige and G. Amarasuriya, "Cell-free massive MIMO with underlay spectrum-sharing," in *IEEE Int. Conf. Commun. (ICC)*, pp. 1–7, May 2019.

[11] Z. Dai, R. Li, J. Xu, Y. Zeng, and S. Jin, "Rate-region characterization and channel estimation for cell-free symbiotic radio communications," *IEEE Trans. Commun.*, vol. 71, pp. 674–687, Feb. 2023.

[12] X. Jia and X. Zhou, "Power beacon placement for maximizing guaranteed coverage in bistatic backscatter networks," *IEEE Trans. Commun.*, vol. 69, pp. 7895–7909, Nov. 2021.

[13] Z. Dai, R. Li, J. Xu, Y. Zeng, and S. Jin, "Cell-free symbiotic radio: Channel estimation method and achievable rate analysis," in *IEEE/CIC Int. Conf. Commun. in China (ICCC Workshops)*, pp. 25–30, Jul. 2021.

[14] K. Han and K. Huang, "Wirelessly powered backscatter communication networks: Modeling, coverage, and capacity," *IEEE Trans. Wireless Commun.*, vol. 16, pp. 2548–2561, Apr. 2017.

[15] F. Rezaei, D. Galappaththige, C. Tellambura, and A. Maaref, "Time-spread pilot-based channel estimation for backscatter networks," *IEEE Trans. Commun.*, vol. 72, pp. 434–449, Jan. 2024.

[16] M. Hua, L. Yang, C. Li, Z. Zhu, and I. Lee, "Bistatic backscatter communication: Shunt network design," *IEEE Internet Things J.*, vol. 8, pp. 7691–7705, May 2021.

[17] A. Kaplan, J. Vieira, and E. G. Larsson, "Dynamic range improvement in bistatic backscatter communication using distributed MIMO," in *IEEE Global Commun. Conf.*, pp. 2486–2492, Dec. 2022.

[18] Q. Tao, Y. Li, C. Zhong, S. Shao, and Z. Zhang, "A novel interference cancellation scheme for bistatic backscatter communication systems," *IEEE Commun. Lett.*, vol. 25, pp. 2014–2018, Jun. 2021.

[19] G. Sacarelo, M. Awais, and Y. H. Kim, "Bistatic backscatter NOMA with transmit and receive beamforming," in *Int. Conf. Inf. Commun. Techn. Converg. (ICTC)*, pp. 851–853, Oct. 2021.

[20] H. Yang, Y. Ye, K. Liang, and X. Chu, "Power beacon energy consumption minimization in wireless powered backscatter communication networks," *Early Access*, Apr. 2023.

[21] H. Yang, Y. Ye, and X. Chu, "Max-min energy-efficient resource allocation for wireless powered backscatter networks," *IEEE Wireless Communications Letters*, vol. 9, pp. 688–692, May 2020.

[22] X. Wang, H. Yiğitler, and R. Jäntti, "Gaining from multiple ambient sources: Signaling matrix for multi-antenna backscatter devices," *IEEE Wireless Commun. Lett.*, vol. 12, pp. 491–495, Mar. 2023.

[23] L. Qu, D. Mishra, and J. Yuan, "Channel estimation protocol for bistatic backscattering using multiantenna transceiver," in *IEEE 33rd Annual Int. Symposium on Personal, Indoor and Mobile Radio Commun. (PIMRC)*, pp. 439–444, Sept. 2022.

[24] M. Yerzhanova and Y. H. Kim, "Channel estimation via model and learning for monostatic multiantenna backscatter communication," *IEEE Access*, vol. 9, pp. 165341–165350, Dec. 2021.

[25] M. Mohammadi, Z. Mobini, D. Galappaththige, and C. Tellambura, "A comprehensive survey on full-duplex communication: Current solutions, future trends, and open issues," *IEEE Commun. Surveys Tuts.*, vol. 25, pp. 2190–2244, 4th Quat. 2023.

[26] Y. Liao, G. Yang, and Y.-C. Liang, "Resource allocation in NOMA-enhanced full-duplex symbiotic radio networks," *IEEE Access*, vol. 8, pp. 22709–22720, Jan. 2020.

[27] G. Yang, D. Yuan, Y.-C. Liang, R. Zhang, and V. C. M. Leung, "Optimal resource allocation in full-duplex ambient backscatter communication networks for wireless-powered IoT," *IEEE Internet Things J.*, vol. 6, pp. 2612–2625, Apr. 2019.

[28] Ö. Demir, E. Björnson, and L. Sanguinetti, *Foundations of User-Centric Cell-Free Massive MIMO*. Foundations and trends in signal processing, Now Publishers, 2021.

[29] W. Zhao, G. Wang, S. Atapattu, T. A. Tsiftsis, and X. Ma, "Performance analysis of large intelligent surface aided backscatter communication systems," *IEEE Wireless Commun. Lett.*, vol. 9, pp. 962–966, Feb. 2020.

[30] L. Yang, Y. Yang, M. O. Hasna, and M.-S. Alouini, "Coverage, probability of SNR gain, and DOR analysis of RIS-aided communication systems," *IEEE Commun. Lett.*, vol. 9, pp. 1268–1272, Aug. 2020.

[31] W. Zhao, G. Wang, B. Ai, J. Li, and C. Tellambura, "Backscatter aided wireless communications on high-speed rails: Capacity analysis and transceiver design," *IEEE J. Sel. Areas Commun.*, vol. 38, pp. 2864–2874, Dec. 2020.

[32] J. Wu and P. Fan, "A survey on high mobility wireless communications: Challenges, opportunities and solutions," *IEEE Access*, vol. 4, pp. 450–476, Jan. 2016.

[33] D. Galappaththige, F. Rezaei, C. Tellambura, and S. Herath, "RIS-empowered ambient backscatter communication systems," *IEEE Wireless Commun. Lett.*, vol. 12, pp. 173–177, Jan. 2023.

[34] D. Wang, F. Rezaei, and C. Tellambura, "Performance analysis and resource allocations for a WPCN with a new nonlinear energy harvester model," *IEEE open j. Commun. Soc.*, vol. 1, pp. 1403–1424, Sept. 2020.

[35] D. Galappaththige and G. Aruma Baduge, "Exploiting distributed IRSs for enabling SWIPT," *IEEE Wireless Commun. Lett.*, vol. 11, pp. 673–677, Apr. 2022.

[36] R. Long, Y.-C. Liang, H. Guo, G. Yang, and R. Zhang, "Symbiotic radio: A new communication paradigm for passive internet of things," *IEEE Internet Things J.*, vol. 7, pp. 1350–1363, Feb. 2020.

[37] D. Tse and P. Viswanath, *Fundamentals of Wireless Communication*. Cambridge University Press, 2005.

[38] S. M. Kay, *Fundamentals of statistical signal processing: estimation theory*. Prentice-Hall, Inc., 1993.

[39] Q. Zhang, S. Jin, K.-K. Wong, H. Zhu, and M. Matthaiou, "Power scaling of uplink massive MIMO systems with arbitrary-rank channel means," *IEEE J. Sel. Topics Signal Process.*, vol. 8, pp. 966–981, Oct. 2014.

[40] H. Q. Ngo, A. Ashikhmin, H. Yang, E. G. Larsson, and T. L. Marzetta, "Cell-free massive MIMO versus small cells," *IEEE Trans. Wireless Commun.*, vol. 16, pp. 1834–1850, Mar. 2017.

[41] "Positioning techniques for mobile devices in LTE," Jul. 2015. Available Online: https://www.hsc.com/resources/blog/positioning-techniques-for-mobile-devices-in-lte/.

[42] S. Stanczak, M. Wiczanowski, and H. Boche, *Fundamentals of Resource Allocation in Wireless Networks: Theory and Algorithms*. Springer Publishing Company, Incorporated, 2nd ed., 2009.

[43] K. Shen and W. Yu, "Fractional programming for communication systems—part I: Power control and beamforming," *IEEE Trans. Signal Process.*, vol. 66, pp. 2616–2630, May 2018.

[44] D. Galappaththige, D. Kudathanthirige, G. Amarasuriya, and C. Tellambura, "Weighted sum-rate maximization for distributed RIS-assisted cell-free massive MIMO," in *IEEE Conf. Standards for Commun. Netw. (CSCN)*, pp. 236–241, Nov. 2022.

[45] S. Boyd and L. Vandenberghe, *Convex Optimization*. Cambridge University Press, Mar. 2004.

[46] K. Shen, *Fractional Programming for Communication System Design*. Phd thesis, University of Toronto, Ontario, Canada, June 2020. Available at https://tspace.library.utoronto.ca/handle/1807/101285.

[47] S. Stanczak, *Fundamentals of Resource Allocation in Wireless Networks Theory and Algorithms*. Berlin, Heidelberg: Springer Berlin Heidelberg, 2nd ed., 2008.

[48] W. Wan, X. Wang, J. Yang, and B. Zhao, "Joint linear pre-coder and combiner optimization for distributed antenna systems," in *IEEE Global Commun. Conf. (GLOBECOM)*, pp. 1–6, Dec. 2016.

[49] H. Guo, Y.-C. Liang, J. Chen, and E. G. Larsson, "Weighted sum-rate maximization for intelligent reflecting surface enhanced wireless networks," in *Global Commun. Conf. (GLOBECOM)*, pp. 1–6, Dec. 2019.

[50] Q. Wu and R. Zhang, "Intelligent reflecting surface enhanced wireless network via joint active and passive beamforming," *IEEE Trans. Wireless Commun.*, vol. 18, pp. 5394–5409, Nov. 2019.

[51] J. S. Borrero, C. Gillen, and O. A. Prokopyev, "Fractional 0—1 programming: Applications and algorithms," *J. of Global Optimization*, vol. 69, pp. 255–282, Sept. 2017.

[52] J. C. Bezdek and R. J. Hathaway, "Convergence of alternating optimization," vol. 11, Dec. 2003.

[53] A. Ben-Tal and A. S. Nemirovskiaei, *Lectures on Modern Convex Optimization: Analysis, Algorithms, and Engineering Applications*. USA: Soc. Ind. Appl. Math., 2001.

[54] J. Chung, C.-S. Hwang, K. Kim, and Y. K. Kim, "A random beamforming technique in MIMO systems exploiting multiuser diversity," *IEEE J. Sel. Areas Commun.*, vol. 21, pp. 848–855, Jun. 2003.

[55] M. Sharif and B. Hassibi, "On the capacity of MIMO broadcast channel with partial side information," in *Proc. 37 Asilomar Conf. Signals, Systems & Computers*, vol. 1, pp. 958–962, Nov. 2003.

Diluka Galappaththige (S'17–M'22) is a postdoctoral research fellow at the Department of Electrical and Computer Engineering, University of Alberta, Canada. He received B.Sc. degree (First-class honor) in Electrical and Electronic Engineering from the Department of Electrical and Electronic Engineering, University of Peradeniya, Sri Lanka, in 2017, and a Ph.D. in Electrical and Computer Engineering from the School of Electrical, Computer, and Biomedical Engineering, Southern Illinois University, Carbondale, IL, USA, in 2021.

Dr. Galappaththige has been awarded a post-doctoral fellowship from NSERC for the academic year 2024-2026. His current research interests include but are not limited to, the design, modeling, and analysis of massive multiple-input multiple-output (mMIMO) communication (i.e., including co-located mMIMO and cell-free/distributed mMIMO), full-duplex communication (FD), backscatter communication (BackCom), reconfigurable intelligent surfaces (RISs), integrated sensing and communication (ISAC), wireless power transfer, and emerging technologies for enabling fifth-generation (5G) and beyond wireless networks. He was a recipient of the Exemplary Reviewer Award for IEEE Wireless Communications Letters (TWCL) in 2020, and IEEE Communications Letters (TCL) in 2021. He has actively served as a reviewer for a variety of IEEE journals and conferences, including TCOM, TVT, TGCN, IEEE Access, IEEE Network, TCL, TWCL, ICC, and GLOBCOM.

Fatemeh Rezaei (S'12–M'22) is currently with the Huawei Technologies Canada Research Center (CRC) in Ottawa, ON, working on innovative technologies for advanced 5G and beyond. She received her Ph.D. degree (with distinction) in Electrical Engineering from Yazd University (YU), Iran, in 2021.

Dr. Rezaei served as a Postdoctoral Fellow at the Department of Electrical and Computer Engineering, University of Alberta, Canada, from December 2021 to December 2023. Prior to this, she was a Visiting Researcher at the same department from February 2019 to September 2020. Her current research interests include wireless communications and signal processing for advanced cellular networks, including backscatter communications, Internet of Things (IoT), energy harvesting systems, MIMO and massive MIMO, intelligent reflective surfaces, non-orthogonal multiple access, cognitive radio networks, and machine learning for wireless networks.

Chintha Tellambura (Fellow, IEEE) received the B.Sc. degree (First class) in electrical and electronic engineering from the University of Moratuwa, Sri Lanka, the M.Sc. degree in electrical engineering from King's College, University of London, and the Ph.D. degree in electrical engineering from the University of Victoria, Canada. He was with Monash University, Australia, from 1997 to 2002. Dr. Tellambura is a Professor in the Department of Electrical and Computer Engineering at the University of Alberta. He has authored or co-authored over 600 journals and conference papers, demonstrating his expertise in the field. According to Google Scholar, his exceptional scholarly contributions have earned him an impressive H-index of 84. Dr. Tellambura has made significant contributions to various areas of research, including future wireless networks, machine learning for wireless networks, and signal processing.

Recognizing his outstanding accomplishments, he was elected as an IEEE Fellow in 2011 for his noteworthy contributions to physical layer wireless communication theory. In 2017, he was further honored as a fellow of the Canadian Academy of Engineering, a testament to his exceptional achievements. His dedication and expertise have been acknowledged through prestigious awards, including the Best Paper Awards in the Communication Theory Symposium in 2012, the IEEE International Conference on Communications (ICC) held in Canada in 2017, and another ICC in France. Moreover, Dr. Tellambura has been honored with the esteemed McCalla Professorship and the Killam Annual Professorship by the University of Alberta, further underscoring his significant impact on academia. Dr. Tellambura has also played a vital role in editorial responsibilities within the IEEE community. He served as an Editor for the IEEE Transactions on Communications from 1999 to 2011 and for the IEEE Transactions on Wireless Communications from 2001 to 2007. In the latter role, he was Area Editor of Wireless Communications Systems and Theory from 2007 to 2012, contributing to advancing the field through his editorial expertise.

Amine Maaref received the Ph.D. degree in telecommunications from INRS, Quebec University, in 2007. Since 2011 he has been with the Huawei Technologies Canada Research Center (CRC) in Ottawa, ON, where he currently holds the position of Senior Principal Engineer, focusing on 5G/6G radio access design. He is an LTE and NR technical expert and has been part of Huawei Technologies 3GPP RAN1 standard delegation, during which time he was actively involved in 5G NR Release 15/16 standardization. Prior to joining Huawei, he was with Mitsubishi Electric Research Labs (MERL), in Cambridge, MA, USA, as a Research Scientist, where he conducted advanced research in broadband mobile communications and was actively involved in 3GPP LTE/LTE-Advanced and WiMAX IEEE 802.16m standardization.

Over the last 20 years, he has co-authored more than 100 international peer-reviewed publications and standard contributions in the relevant fora, holds more than 350 worldwide awarded patents and pending patent applications, and received numerous prestigious awards for his outstanding research and scholarly achievements. He was the Guest Editor for several special issues of IEEE journals and magazines and was the founding Managing Editor of IEEE 5G/Future Networks Tech Focus. From 2014 to 2020, he served as an Editor of the IEEE Transactions on Wireless Communications and currently serves as an Editor of IEEE Transactions on Communications.